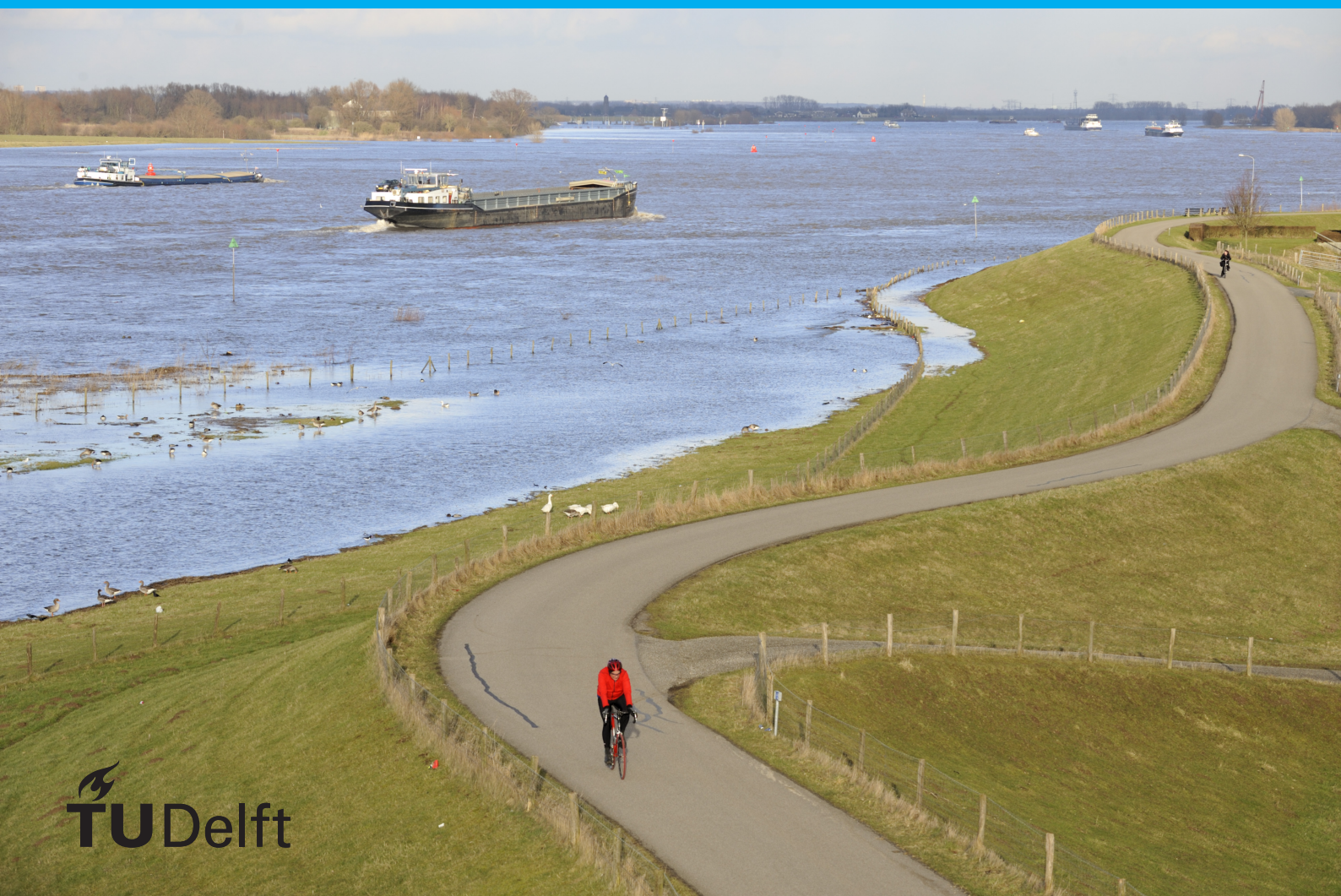


Quantification of the Uncertainty in river discharges due to Climate Change

And the consequences for flood protection designs in The Netherlands

D.J.P. Wubben



Quantification of the Uncertainty in river discharges due to Climate Change

And the consequences for flood protection designs in The
Netherlands

by

D.J.P. Wubben

to obtain the degree of Master of Science
at the Delft University of Technology,
to be defended publicly on Thursday July 19, 2018 at 16:00.

Student number:	4321340	
Project duration:	June 2017 – July 2018	
Thesis committee:	Prof. dr. ir. M. Kok,	TU Delft, supervisor
	Dr. ir. W. Kanning,	TU Delft
	Dr. ir. S. van Vuren,	TU Delft
	Dr. J.J. Beersma,	KNMI
	Dr. ir. R. Vos,	Rijkswaterstaat

An electronic version of this thesis is available at <http://repository.tudelft.nl/>.

Cover picture: *Hoogwater Waal met zicht op dijk*, Martin van Lokven (source:
<http://beeldbank.rws.nl/>)

Preface

This report is established with the help of a couple of people. Without these people the report would never be as it is now. I would like to take the opportunity to thank these people for their help.

First of all, I would like to thank all the members of the graduation committee. Professor Matthijs Kok for leading the committee, his guidance during the whole process and his feedback. Wim Kanning for his help with finding and formulating a research topic, guidance to structure the report and feedback. Saskia van Vuuren and Robert Vos for their helpful feedback and explanations of some subjects. And Jules Beersma, who always found time for me, to explain, comment and discuss all the subjects of the report.

Furthermore, I would like the KNMI for providing the subject and their facilities. In particular I would like to thank Adri Buishand for spending many hours on commenting the report. Due to his critical look the report has improved a lot. The knowledge of Jules and Adri learned me a lot about climate science.

I also want to thank Mark Hegnauer from Deltares for providing the river simulation data, explanation about the GRADE instrument and discussion of the results. And I thank Hendrik Buiteveld from Rijkswaterstaat for the discussion of the results during the fruitful meetings.

And last I would like to thank my family, friends and other students for their help en support during the study and thesis work. Their support helped me allot during though times in the process.

*Dennis Wubben
Delft, July 2018*

Summary

The Earth's climate system is changing due to increased greenhouse gas concentrations in the atmosphere. The development of the future climate is, however, very uncertain. This uncertainty is caused by a lack of knowledge of the Earth's climate system and of future emissions of greenhouse gasses into the atmosphere. Due to climate change more extreme rainfall events are expected and these events have an impact on the (extreme) river discharges. The uncertainties in the future climate cause uncertainty in the projections of the future extreme river discharges. For flood protection considerations, it is important to quantify the climate uncertainties and its effects on extreme river discharges.

Projections of future changes in the climate system are typically obtained from simulations with Global Climate Models (GCMs). These GCMs are driven by future greenhouse gas concentrations. For a better comparison between various studies the IPCC (International Panel on Climate Change) constructed so-called Representative Concentration Pathways (RCPs), which are pre-defined forcing paths in time. The IPCC has selected four different RCPs that largely span the future range in greenhouse gas concentrations. The RCPs have a radiative forcing target level for 2100 of 2.6, 4.5, 6.0 and 8.5 W/m² (at top of the atmosphere) and are therefore named; RCP2.6, RCP4.5, RCP6.0 and RCP8.5, respectively. RCP2.6 is a mitigation scenario, RCP4.5 and RCP6.0 are two medium stabilization scenarios and RCP8.5 is a business-as-usual scenario.

For the Netherlands the Royal Netherlands Meteorological Institute (KNMI) constructed climate change scenarios based on GCM projections. The four KNMI'14 climate scenarios were set up by a two-axis framework. One axis expresses the change in the projected global mean temperature and the other axis represents the change in the large scale atmospheric flow, which largely determines the precipitation in and around The Netherlands. This two-axis framework is expressed in the name of the scenarios. The so-called G-scenarios presume a relatively small increase in global mean temperature and the W-scenarios presume a stronger temperature increase. The subscript H represents a strong precipitation change and the subscript L a weak(er) in precipitation response.

In this study the uncertainties in the discharges of the river Rhine in the Netherlands resulting from uncertainties in the future climate are considered and the consequences of these uncertainties for flood protection designs. Time series of daily precipitation and temperature of the Rhine basin are transformed into representative time series for the climate of 2085 using the changes in the KNMI'14 climate scenarios and GCM simulations.

The GRADE (Generator of Rainfall and Discharge Extremes) instrument has been developed for the Rhine basin to obtain a time series of daily river discharges from daily precipitation and temperature data. This instrument consists of three components. First, a stochastic weather generator that produces very long daily precipitation and temperature series by sampling from much shorter series. Secondly, a hydrological model (HBV) that transforms the precipitation and temperature series into river discharges. Thirdly, a hydrodynamic model (Sobek) is used to simulate the routing of the largest flood waves. GRADE simulations usually consist of 50,000 years which make these simulations computationally expensive.

GRADE was already used in combination with the four KNMI'14 scenarios. And although these four scenarios cover a considerable part of the climate change uncertainty, they do not cover it fully. To be able to determine the uncertainties in future river discharges more extensively, a large number of river discharge simulations based on various GCM projections is needed. GRADE is however computationally too expensive for this purpose. Alternatively much shorter, i.e. 56-year, future river discharge simulations with the HBV model were performed, based on the precipitation and temperature changes in the CMIP5 (Coupled Model Intercomparison Project phase 5) climate model simulations. In this thesis both these short CMIP5 based discharge simulations and the long KNMI'14 based HBV simulations from the GRADE instrument are used. The CMIP5 ensemble consists of 183 climate model simulations, conducted with 29 different GCMs and driven by the four RCPs. Although this is a sufficient amount of climate model simulations, the river simulations

were only made for a time series of 56 years, which is not sufficient to determine the uncertainties in extreme discharge return levels. The CMIP5 based discharge simulations are just used to determine the uncertainties in the change in mean annual maximum discharge (dMHQ).

To assess the uncertainties in the extreme discharge return levels subsequently, relations between the dMHQ and the changes in the T-year return levels (dHQ_T) are used. These relations are obtained with the GRADE discharge simulations based on the KNMI'14 climate scenarios. From these simulations 50,000 annual maximum discharges were available, which is sufficient to determine the extreme return levels. For the relation between dMHQ and dHQ_T a linear relation, forced through the origin, is used. The slope of this linear relation increases with the return period and thus each return level has its own relation.

For the quantification of the sources of uncertainty in the dMHQ's of the CMIP5 simulations use is made of a Linear Mixed-Effects (LME) model. An LME-model is an ANOVA (Analysis of Variance) model that includes fixed effects and random effects. The LME-model describes the variation in dMHQ as a function of the forcing, climate model uncertainty and natural variability. The LME-model that fits the data of the 183 CMIP5 simulations best is a single-level mixed effects model with a fixed effect of the forcing, an interaction between a random climate model effect and the forcing, and a random error representing the influence of natural variability on dMHQ.

This LME-model is used as starting point for the determination of the uncertainties in the extreme discharge return levels. For a specific return level and RCP forcing first, a random dMHQ is generated from the LME-model (without the random error representing natural variability). Second, this dMHQ is converted into dHQ_T with the relation between dMHQ and dHQ_T for that return level. Third, the value of dHQ_T is added to HQ_T for the present climate, to obtain HQ_T for the future climate. Subsequently, a random value is drawn from the normal distribution representing natural variability and HBV parameter (i.e. hydrological) uncertainty for that return level and added to the value of HQ_T . And finally, this hydrological (HBV) discharge is converted into a hydrodynamic (Sobek) discharge with a relation between HBV and Sobek discharges from a GRADE simulation based on earlier KNMI climate scenario. With a sufficient number of realizations a distribution of the discharge of that specific return level and RCP scenario can be constructed. These steps are repeated for various return levels and the four RCP scenarios. The distributions of the various return levels are combined to a discharge frequency curve per RCP scenario with a 95% confidence band.

In all KNMI'14 scenario and RCP based discharge simulations of the Rhine at Lobith for 2085 there is a systematic increase of the discharge return levels. For the 10,000-year return level the difference between the means for RCP8.5 and RCP2.6 of $788 \text{ m}^3/\text{s}$ can be seen as the forcing scenario uncertainty. For a given RCP scenario there is an uncertainty in the return levels due to natural variability, hydrological uncertainty and climate model uncertainty. The uncertainty due to natural variability and hydrological uncertainty also exists for the reference situation. The difference in width of the 95% confidence interval of the RCP scenarios and the reference situation is the additional uncertainty caused by the different climate model responses to an RCP scenario. For the 10,000-year return level this difference is 82, 279, 445 and $1000 \text{ m}^3/\text{s}$ for RCP2.6, RCP4.5, RCP6.0 and RCP8.5, respectively. So for this return level the mean difference in response to the range in RCP forcings of $788 \text{ m}^3/\text{s}$ is of similar order (in fact somewhat smaller) than increase in the uncertainty of $1000 \text{ m}^3/\text{s}$ for RCP8.5 due to climate model response uncertainty.

The range spanned by the four KNMI'14 scenarios for 2085 best corresponds with the width of the 95% confidence range for the RCP8.5 scenario. However, for the 10,000-year return level the width of the 95% confidence region of RCP8.5 becomes much larger than the range described by the KNMI'14 scenarios. For the other three RCP scenarios the KNMI'14 scenarios are mainly located in the upper half of the 95% confidence interval. This indicates that there is more than 50% chance that the KNMI'14 scenarios will never be exceeded in 2085 in these RCP scenarios.

The uncertainties in future extreme river discharges due to climate change have consequences for the water levels used for dike designs. In this study the consequences are only considered for the design water levels for the failure mechanism overtopping at four different locations along the Rhine. This water level gives a good indication of the relative influence of climate change on water levels for the dike designs.

The design water level for the failure mechanism overtopping is, in good approximation, equal to the water level with a return period equal to the safety standard of the dike section. For the determination of the uncertainties in the design water level for a specific RCP scenario and location first a random discharge is drawn from the discharge distribution of the RCP scenario with a return level equal to the safety standard of the location. Subsequently, this discharge is converted into a water level by a relation between the river discharge at Lobith (Q) and the local water level (h), the Q - h relation. With a sufficient number of realizations a distribution of the design water level of that specific location and RCP scenario can be constructed. These steps are repeated for the four RCP scenarios and the four locations.

The first location considered is situated along the Waal and part of dike section 42-1, which has a safety standard of 1/10,000 per year. At this location the mean values of the design water level are 15.53, 15.60, 15.63 and 15.75 m for RCP2.6, RCP4.5, RCP6.0 and RCP8.5, respectively. The mean of the reference situation at this location is 15.24 m, so there is an increase of 0.29 - 0.51 m for the design water level due to the RCP forcing. The standard deviation of the design water level for the RCP scenarios is in the range of 0.25 - 0.30 m, which is of the same order as the range in the increase in the mean value for the RCP scenarios. For the other three locations the range in the increase in the mean value is of the same order, the difference between RCP8.5 and RCP2.6 is about 0.2 m. And also the standard deviations of each RCP scenario is in the same order.

Integration of the uncertainties in the discharge frequency curve lead to an increase of the design water level of 0.08 to 0.13 m (depending on the RCP scenario) with respect to the mean value of the design water level distributions per RCP scenario. This increase is somewhat different for the four locations along the Rhine. When the results are compared for the location along the Waal (Location 1) for the RCP scenarios with the reference situation, the design water level is 0.29 - 0.51 m higher due to the four RCP scenario forcings and above this water level an additional height of 0.09 - 0.12 m is required for the uncertainties within an RCP scenario.

The design water level based on the KNMI'14 scenarios is only considered for the location along the Waal (dike section 42-1). The design water level, with the uncertainties integrated, becomes 15.60, 15.82, 16.11 and 15.91 m for 2085GH, 2085GL, 2085WH and 2085WL, respectively. The design water level for the lowest KNMI'14 scenario (2085GH) is almost equal to the 15.62 m for the lowest RCP scenario (RCP2.6). And the design water level for the highest KNMI'14 scenario (2085WH) is 0.26 m higher than the 15.85 m for the highest RCP scenario (RCP8.5). The design water level for the RCP8.5 scenario corresponds most closely to the one for the KNMI'14 2085GL scenario.

This study shows that both the RCP scenario forcing and the uncertainty in the discharge return levels lead to an increase of a few decimetres in the design water level.

Contents

1	Introduction	1
1.1	Problem analysis	1
1.2	Research goals	2
1.3	Research questions	2
1.4	Study area.	3
2	Climate Change	5
2.1	Key concepts in Climate Science	5
2.2	Observed Changes in the Climate System	6
2.3	Climate Modelling	8
2.3.1	Representative Concentration Pathway	8
2.3.2	CMIP5 Climate Model simulations.	8
2.3.3	Future changes in the Rhine basin	10
2.3.4	KNMI Climate Scenarios	13
2.4	Modelling from meteorology to river discharge	15
2.4.1	Stochastic weather generator	15
2.4.2	Hydrological modelling	16
2.4.3	Flood routing	16
3	Uncertainties in future River discharges	19
3.1	Long time series.	21
3.1.1	KNMI'14 projections.	21
3.1.2	Relation dMHQ - dHQ	22
3.2	Short time series	23
3.2.1	Quantification of the sources of uncertainty	23
3.2.2	Change in mean annual maximum discharge	29
3.3	HBV discharge projections	30
3.3.1	Annual maximum discharge	30
3.3.2	HBV discharge frequency curves.	31
3.4	Sobek discharge projections	33
3.4.1	HBV-Sobek relation	34
3.4.2	Hydraulic uncertainty	35
3.4.3	Sobek discharge frequency curves	37
3.4.4	Comparison of the RCP PDFs with the KNMI'14 scenarios.	38
4	Consequences of the climate uncertainties for the Dike Designs	41
4.1	Flood protection system in The Netherlands	41
4.1.1	History.	41
4.1.2	Overview.	42
4.1.3	Safety Standards	42
4.2	Basic concepts of Flood Defences.	45
4.2.1	Dike profile	45
4.2.2	Failure mechanisms	45
4.3	Method to determine the design water level for overtopping	47
4.4	Uncertainty in design water level	50
4.5	Design water level with integrated uncertainties	51
4.5.1	Method to integrate the uncertainty	51
4.5.2	Discharge frequency curves with integrated uncertainties	52
4.5.3	Results for Location 1	52
4.5.4	Results for the other locations	52

4.6	Comparison of design water level with the KNMI'14 climate scenarios	54
5	Discussion	57
5.1	Regression lines.	57
5.2	The consequences of the climate uncertainties on design water levels	59
6	Conclusions and Recommendations	61
6.1	Conclusions.	61
6.2	Recommendations	63
	Bibliography	65

Introduction

1.1. Problem analysis

The causes and effects of climate change are hot topics at the moment. Many studies show the existence of climate change [12]. There is a widespread consensus about the existence of climate change, due to increased greenhouse gas (carbon dioxide (CO_2), methane (CH_4), Nitrous Oxide (N_2O), etc.) concentrations in the atmosphere, but there is much uncertainty about the development of the future climate.

The Earth's climate system is very complex and still not fully understood. This lack of knowledge causes a large uncertainty in the predictions of the future development of the climate on Earth. Another source of uncertainty is the emission of greenhouse gasses in the atmosphere. Greenhouse gas emissions largely depend on the development of new technologies and mitigation politics. This makes it hard to predict the future greenhouse gas concentrations in the atmosphere, and it also makes the predictions of the future climate uncertain.

Due to climate change the sea level rises and more extreme rainfall events occur. Changes in rainfall have an impact on river discharges. The future sea level and river discharges therefore depend on the future climate. These quantities are important for the flood protection system in The Netherlands. The dike reinforcements programs make use of projections of the future sea level and river discharges. Due to the uncertainties in the future climate these projections are also uncertain. These uncertainties need to be taken into account in the flood protection designs and therefore it is important to know the magnitude of the uncertainties due to climate change. In an earlier research this is already done for the sea level near the Dutch coast [27]. The uncertainties in extreme river discharges of the Dutch rivers due to climate change are however not fully known.

For flood protection designs the current Dutch guideline makes use of the KNMI'14 climate scenarios. This set of four scenarios is developed by the Royal Netherlands Meteorological Institute (KNMI) and describes possible ways of the climate development in The Netherlands [17]. In the flood protection guideline the KNMI scenario is used that leads to the most extreme river discharges. Uncertainties in this scenario are taken into account by an additional discharge.

Future discharges of the main rivers in The Netherlands have been simulated for each of the KNMI'14 scenarios [29]. The spread in the return levels of the extreme discharges gives an indication of the magnitude of the uncertainties. For good dike design considerations it is important to know the uncertainties in the future river discharges better.

1.2. Research goals

The first goal of this research is to determine the uncertainties in the river discharges due to climate change. We then assess how for the extreme river discharges under the KNMI scenarios cover the spread in the discharges due to the climate change uncertainties.

The second goal is to determine the consequences of these uncertainties for dike design considerations. For this goal a range in the dimensions of a dike due to uncertainties in the river discharges has to be determined and a method to include these uncertainties in the dike design has to be found.

1.3. Research questions

Below the research questions for this research are formulated. There are three main questions, of which the first is divided into two sub questions.

1. How large are the uncertainties in the future extreme river discharges due to climate change and what are the consequences of these uncertainties for flood protection designs in The Netherlands?

For this question the two sub questions are:

1a. How large is the uncertainty in the extreme discharge of the Rhine at Lobith due to climate change uncertainties for different discharge return levels?

1b. What are the consequences of the climate change uncertainties on the local water level corresponding to the safety standard?

2. How are the discharge return levels for the four KNMI'14 climate scenarios situated in the probability distributions of the discharge return levels based on a large number of climate model simulations?

3. How do the results of this study compare to the currently used KNMI'14 scenarios.

1.4. Study area

This study focusses on the upper part of the Rhine in The Netherlands. The water levels in this part of the river depend only on the river discharge and not on the sea level.

The Rhine is, with a total length of 1230 km, the longest river in North Western Europe. The river originates in the Swiss Alps and empties in the North Sea in The Netherlands. The basin with a catchment area of 185,000 km² is situated in nine countries. The average discharge at Lobith is 2200 m³/s and the river is fed by rainfall, snow melt and glacier melt.

Lobith is the location where the river Rhine enters the Netherlands. The river discharges at this location are used for the flood protection designs in The Netherlands. In this study the river discharges are also considered for this location.

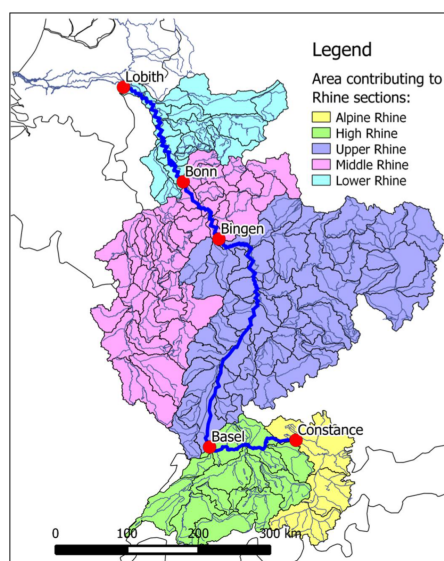


Figure 1.1: Overview of the Rhine basin (source: [9])

Extreme floods in the Lower Rhine typically occur in the winter and early spring (November - April). These are caused by a combination of multi-day precipitation over a large area, saturated soils, and little evaporation. Frozen soils and snow melt may enhance the occurrence of extreme run off.

2

Climate Change

2.1. Key concepts in Climate Science

The terms weather and climate are often used interchangeably, while they essentially mean something different. Therefore, it's important to distinguish the meaning of weather from climate. Weather describes the atmospheric condition at a certain place and time, with reference to parameters as temperature, pressure, humidity and wind. But weather also describes the presence of clouds, precipitation, storms, etcetera. The weather is generally described in short time frames, minutes to weeks. Climate is usually defined as the average weather over a period of 30 years. But it is better to define it as the statistical description in terms of the mean and variability of relevant quantities. The relevant quantities are most often surface variables such as temperature, precipitation and wind. The statistics for climate also describes the associated statistics (frequency, magnitude, persistence, trends, etc.) of combining parameters. Climate change refers to a significant change of the statistical climate distribution, which can be changes in the mean and/or the variability. (IPCC, [3])

The Earth's climate system (as shown in Figure 2.1) is forced by solar radiation from the Sun . About half of the incoming solar shortwave radiation (SWR) is absorbed by the Earth's surface. The rest is absorbed or reflected by climate drivers, such as greenhouse gasses, aerosols (tiny dust particles in the atmosphere), clouds and surface albedo (a measure for sunlight reflection). The absorbed radiation by the Earth's surface is later emitted as long wave radiation (LWR). Most of the outgoing LWR is absorbed by certain climate drivers, and later emit to all directions. The downward component of this LWR adds heat to the lower layers of the atmosphere and the Earth's surface, this is the so called greenhouse effect. When the incoming solar energy is nearly equal to the outgoing radiation, the temperature on Earth remains constant. This applies when there is an energy balance in the Earth's climate system. (IPCC, [3])

Climate change is caused by changes in the global energy budget. This can be changes in either the incoming solar radiation or the outgoing longwave radiation. Changes in the net incoming solar radiation derive from changes in the Sun's output of energy or the Earth's surface albedo. Changes in the outgoing longwave radiation can result from changes in the temperature of the Earth's surface or atmosphere or changes in emissivity of LWR from either the atmosphere or the Earth's surface. Changes in emissivity for the atmosphere are predominantly caused by changes in clouds, greenhouse gases (GHGs) and aerosol concentrations. Humans influence the greenhouse gas [carbon dioxide (CO₂), methane (CH₄), nitrous oxide (N₂O), etc.] and aerosol concentrations by burning fossil fuels. In addition, humans are effecting both the energy and water budget of the planet by changing the land surface. Land use changes change the characteristics of vegetation, including its colour (which effects the surface albedo), seasonal growth (rates of evapotranspiration) and carbon content (reduces carbon storage in the vegetation, adds CO₂ to the atmosphere). Due to the changes induced by humans, the Earth's energy budget is not fully in balance at the moment. (IPCC, [3])

Changes in the atmosphere, land, ocean, biosphere and cryosphere can disturb the Earth's radiation budget, producing a radiative forcing. As a response of this forcing, the Earth's climate system will change. Complex feedback mechanisms ensure that the response of the climate system is not necessarily be proportional

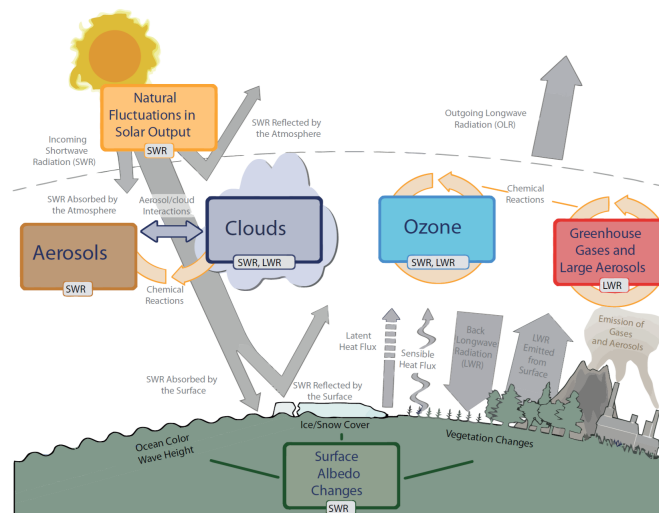


Figure 2.1: Main drivers of Climate Change (source: [3])

to the forcing. The feedback mechanisms can either be positive or negative. An example for a positive feedback is the ice-albedo feedback. When the Earth's temperature increases, snow and ice will melt. Melting ice results in a decrease in surface albedo. Thereby, less solar radiation is reflected and the absorbed radiation in the Earth's surface increases. This results in a further increase of the Earth's temperature. Feedback mechanisms operate on different time scales, ranging from hours to centuries. The different feedback mechanisms, with varying time scales, make it difficult to predict the climate's reaction on the forcings. (IPCC, [3])

2.2. Observed Changes in the Climate System

Observations of the climate system were done since the mid-19th century by direct measurements and remote sensing from satellites. To extend some records back to hundreds or even to millions of years paleoclimate reconstructions were made. The observations and paleoclimate reconstructions together give a comprehensive view of the long-term changes in the atmosphere, ocean, cryosphere and land surface. (IPCC, [13])

For the river discharges the changes in temperature and precipitation are the most important. In Figure 2.2 the observed temperatures in the period 1850 - 2012 are shown. The last three decades have been warmer than any of the earlier decades since 1850. The total increase between the average of the period 1850-1900 and the period 2003-2012 is 0.78 °C, based on the longest dataset available (the Hadley Centre/Climatic Research Unit gridded surface temperature data set 4 (HadCrut4)).

The change in precipitation since 1901 is relatively small before 1951 but considerably increases afterwards (Figure 2.3). The observations show both positive as negative trends in precipitation change. The positive trends were observed in the mid-latitude land areas, especially in the Northern Hemisphere. While the negative trends were observed in dry areas, like the deserts. There is a tendency that dry areas will become drier, while wet areas become wetter.

Other important observed changes are the loss of ice and snow mass, the increase in ocean temperature, the rise of the sea level and the increase in greenhouse gas concentrations in the atmosphere. These are important phenomena for the change in the climate system, but do not influence the river discharges directly. And therefore, these phenomena are not further discussed in this research. The increase in greenhouse gas concentrations in the atmosphere is, however, the main causer of the climate change. Predictions of the future changes in this concentrations are used to predict the future changes in the climate system, which is further described in Section 2.3.

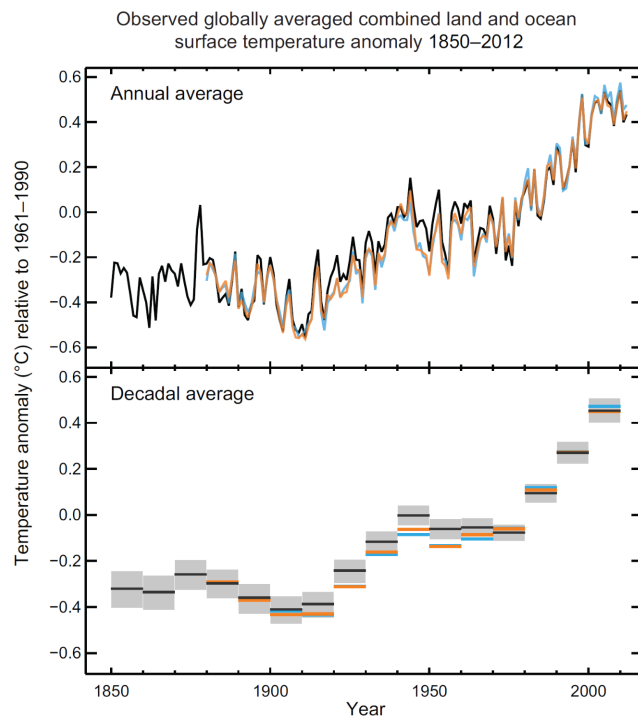


Figure 2.2: Observed global mean combined land and ocean surface temperatures changes, from 1850 to 2012 from three data sets. The data sets of HadCRUT4, MLOST and GISS are used. The top panel shows the annual mean values. The bottom panel shows the decadal mean values, including the estimated uncertainty for one dataset (black line in top panel). The changes are relative to the mean temperature of the period 1961–1990. (source: [13])

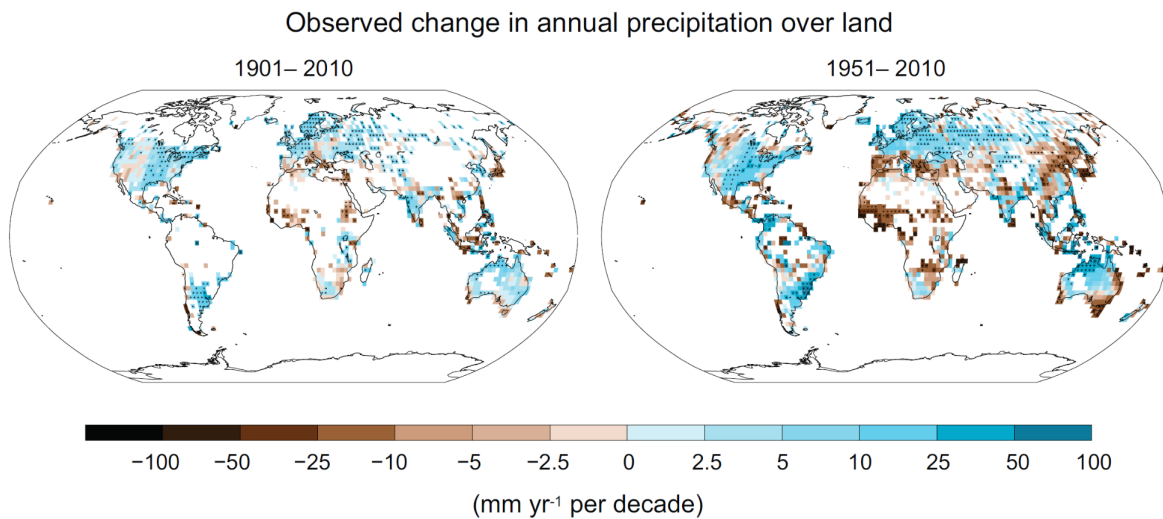


Figure 2.3: Maps of observed precipitation change over land from 1901–2010 and from 1951–2010 from the Global Precipitation Climatology Centre (GPCC) data set. (source: [13])

2.3. Climate Modelling

Projections of future changes in the climate system are typically obtained from simulations with Global Climate Models (GCMs). The future changes depends heavily on the future atmospheric emissions, and consequently concentrations, of greenhouse gases (of which CO₂ is the most known). The development of the greenhouse gases is uncertain since it depends on the size of the world population, the fossil fuel consumption per capita, technological developments and worldwide climate policy measures. It is relatively easy to convert greenhouse gas concentrations into a so-called climate forcing (in W/m²) at the top of the atmosphere where as a result of increased greenhouse gases a new radiation balance is set, resulting in a larger globally averaged temperature near the surface. The second uncertainty involves the amount of globally averaged surface temperature change, which depends on the strengths of the various positive and negative climate feedbacks, given a specified amount of climate forcing. The larger the surface temperature response under a unit amount of climate forcing the larger the so-called climate sensitivity of the GCM. The uncertainty in future greenhouse gas emissions and concentrations can thus be converted into an uncertainty in future climate forcing. The latter is for practical reasons preferred as a starting point for climate model projections. To describe the range in future climate forcings the Intergovernmental Panel on Climate Change (IPCC) constructed so-called Representative Concentration Pathways (RCPs) (see Section 2.3.1 for details).

The GCMs used in this research are described in Section 2.3.2. The results of these GCM simulations have been used to build time series of daily temperature and precipitation for the Rhine basin. The transformation method that is needed for this, is described in Section 2.3.3.

The future changes in The Netherlands are described by climate scenarios constructed by the KNMI. These KNMI climate scenarios were based on the GCM simulations. A description of the scenarios and the construction method is given in Section 2.3.4.

2.3.1. Representative Concentration Pathway

For better comparison between various studies as well as easier communication of model results, it is preferable to use a common set of scenarios. The IPCC Representative Concentration Pathways (RCPs) are a set of emission scenarios adopted by climate modellers to provide a range of possible futures for the evolution of the atmospheric greenhouse gas emissions and concentrations. The RCPs are pre-defined paths of radiative forcing in time (see Figure 2.4), and are used to drive the climate models.

The RCPs include the changes in all major anthropogenic greenhouse gasses. To build the RCPs observed greenhouse gas emissions and concentrations for the historical period (1750-2005) are combined with projected greenhouse gas emissions and concentrations for the period 2005-2100. Due to, the earlier mentioned, climate feedbacks the greenhouse concentrations are somewhat dependent on the resulting future climate, i.e. on the temperature response. Therefore median response characteristics of models assessed in the IPCC Fourth Assessment Report [11] are used. The RCPs are developed until 2100, beyond 2100 the RCPs are extended until 2300 by Extension Concentration Pathways (ECPs). The ECPs are based on the assumption of either smoothly stabilizing concentrations or constant emissions.

IPCC has selected four different RCPs that largely span the future range in greenhouse gas emissions and concentrations. The RCPs are named according to radiative forcing target level for 2100 of 2.6, 4.5, 6.0 and 8.5 W/m² and hence respectively, RCP2.6, RCP4.5, RCP6.0 and RCP8.5. The four selected RCPs include one mitigation scenario leading to a very low forcing level (RCP2.6), two medium stabilization scenarios (RCP4.5 and RCP6.0) and one very high base line emission scenario (RCP8.5). The development of the radiative forcing over time for each RCP is shown in Figure 2.4.

The four scenarios are considered plausible and illustrative, without having probabilities attached to them. More details about the description and construction of the RCPs (and ECPs) can be found in Van Vuuren et al. [32] and Meinshausen et al. [21].

2.3.2. CMIP5 Climate Model simulations

The IPCC Fifth Assessment Report [12] makes use of the CMIP5 (the Coupled Model Intercomparison Project phase 5) climate model simulations. In total the CMIP5 ensemble consists of 200 climate model simulations.

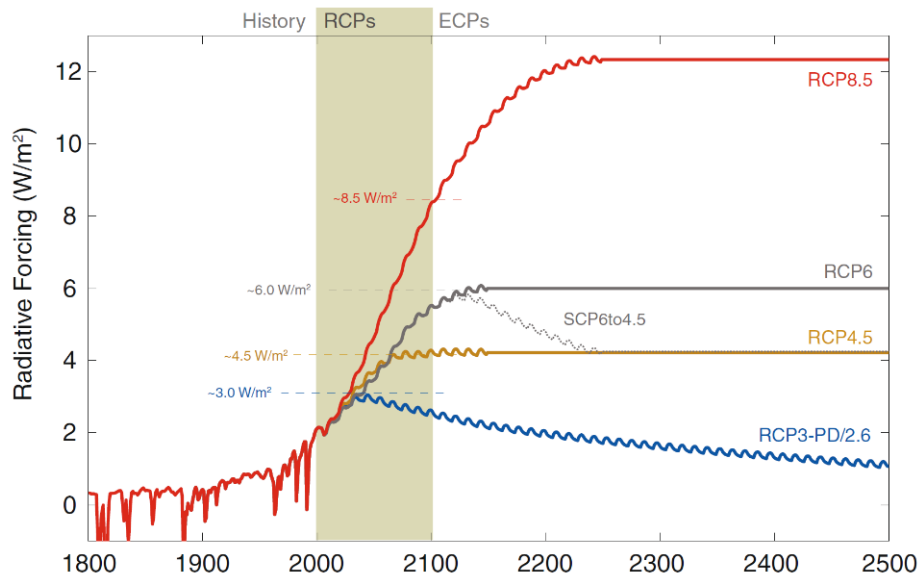


Figure 2.4: Total radiative forcing of the four Representative Concentration Pathways (RCPs) and their Extended Concentration Pathways (ECPs) (source: [21])

For the simulation of river discharges the daily precipitation and temperature are the most important variables. And therefore, only the simulations with both daily precipitation and temperature data for the time-slices 1961-1995, 2021-2050 and 2071-2100 were selected from the available CMIP5 simulations for an earlier river discharge study [29]. The same 183 simulation runs are used again in this research. Table 2.1 gives an overview of this 183 simulations and for each GCM the number of runs per RCP. The 183 simulation runs were conducted with 29 different GCMs. These models are Atmosphere-Ocean General Circulation Models and are, as the name already suggests, a combination of an Atmospheric Circulation Model (ACM) and an ocean model. A number of GCMs uses the same ACM and these GCMs may therefore have similar responses. For this reason the GCMs are also grouped by the ACMs in the later analysis (and also in Table 2.1).

The climate models were driven by the four RCPs. But the four RCPs are not equally represented in the CMIP5 ensemble. While there are 55 simulations forced by the RCP8.5 scenario, the RCP6.0 scenario is only used in 29 simulations. Further, the number of independent simulations performed by a single GCM for a particular RCP varies from 1 to 10. Such independent simulations are constructed by starting the simulations for (slightly) different initial conditions but using exactly the same model configuration and forcing. The difference (in response) between these simulations represent the effect of natural climate variability, which, in turn, is due to the chaotic behaviour of the weather and the climate.

Table 2.1: Overview of the number of climate model runs per Representative Concentration Pathway (RCP) for each Global Climate Model (GCM) used in this study. ACM stands for Atmospheric Circulation Model used in the GCM.

GCM	ACM	RCP				Total
		2.6	4.5	6.0	8.5	
ACCES1-0	HadGEM		1		1	2
ACCES1-3	GA		1		1	2
bcc-csm1-1	BCC	1	1	1	1	4
bcc-csm1-m1	BCC	1	1	1	1	4
BNU-ESM	CAM	1	1		1	3
CanESM2	CanCM	5	5		5	15
CCSM4	CAM	3	3	3	3	12
CMCC-CESM	ECHAM				1	1
CMCC-CM	ECHAM		1		1	2
CMCC-CM5	ECHAM		1		1	2
CNRM-CM5	ARPEGE	1	1		1	3
CSIRO-Mk3-6-0	CSIRO	10	10	10	10	40
GFDL-CM3	GFDL	1		1	1	3
GFDL-ESM2G	GFDL	1	1	1	1	4
GFDL-ESM2M	GFDL	1	1	1	1	4
GISS-E2-R	GISS		1			1
HadGEM2-CC	HadGEM		1		3	4
HadGEM2-ES	HadGEM	4	4	4	4	16
immcm4	INCM		1		1	2
IPSL-CM5A-LR	IPSL	4	4	1	4	13
IPSL-CM5A-MR	IPSL	1	1	1	1	4
IPSL-CM5B-LR	IPSL-B		1		1	2
MIROC5	MIROC	3	3	1	3	10
MIROC-ESM	MIROC	1	1	1	1	4
MIROC-ESM-CHEM	MIROC	1	1	1	1	4
MPI-ESM-LR	ECHAM	3	3		3	9
MPI-ESM-MR	ECHAM	1	3		1	5
MRI-CGCM3	MRI	1	1	1	1	4
NorESM1-M	CAM	1	1	1	1	4
	TOTAL	45	54	29	55	183

2.3.3. Future changes in the Rhine basin

For each of the 183 CMIP5 simulations (Section 2.3.2) the Advanced Delta Change (ADC) method [31] is used to modify (i.e. to transform) historical daily precipitation and temperature time series. These transformed time series are then used to simulate river discharges belonging to that specific future climate (or climate scenario). In the remainder of this section the ADC method is briefly described.

The ADC method was first developed for GCMs from the Coupled Model Intercomparison Project phase 3 (CMIP3) and later extended and applied to the 183 CMIP5 climate model runs mentioned in the previous section [18]. In the ADC method the relative changes in the mean and extreme precipitation can be different, and therefore more consistent with the precipitation responses in the climate model compared to the classical, or ordinary, Delta method in which the relative changes in the mean and extreme precipitation are by definition the same (and therefore potentially at variance with the response in mean and extreme precipitation as indicated by the climate model). Delta change methods are often used because of practical reasons and since they actually avoid the need to correct for biases found in the climate model simulations. But for any Delta change method to work properly it should reproduce the responses in the climate model in the best possible way. In this respect the ADC method is a clear improvement compared to the classical Delta

method. To account for seasonal and spatial differences in the precipitation and temperature differences in the climate model, in the ADC method the precipitation and temperature changes are allowed to vary seasonally and spatially as well.

Precipitation transformation

The first step in the ADC method is to extract the daily precipitation and temperature output of the global climate models from the CMIP5 dataset (see top row of Figure 2.5). Two time-frames are extracted, one for the control period (1961-1995) and one for the future period (either 2021-2050 or 2071-2100). The spatial variation within a GCM is represented by using a (common) grid of grid cells with a resolution of 1.25° latitude and 2.0° longitude.

Extreme river discharges in the Rhine generally result from extreme multi-day precipitation amount in the river area. In other words, it is the change in the statistics of extreme multi-day precipitation that counts and that should be properly represented in the transformed time series. Therefore, ideally the transformation should be based on the response in multi-day precipitation sums rather than on the response of daily precipitation amounts (alone). The statistics of the non-overlapping 5-day sums are therefore considered. The 5-day step recognizes the relevance of multi-day precipitation sums, but is small enough to be linked with daily precipitation as well.

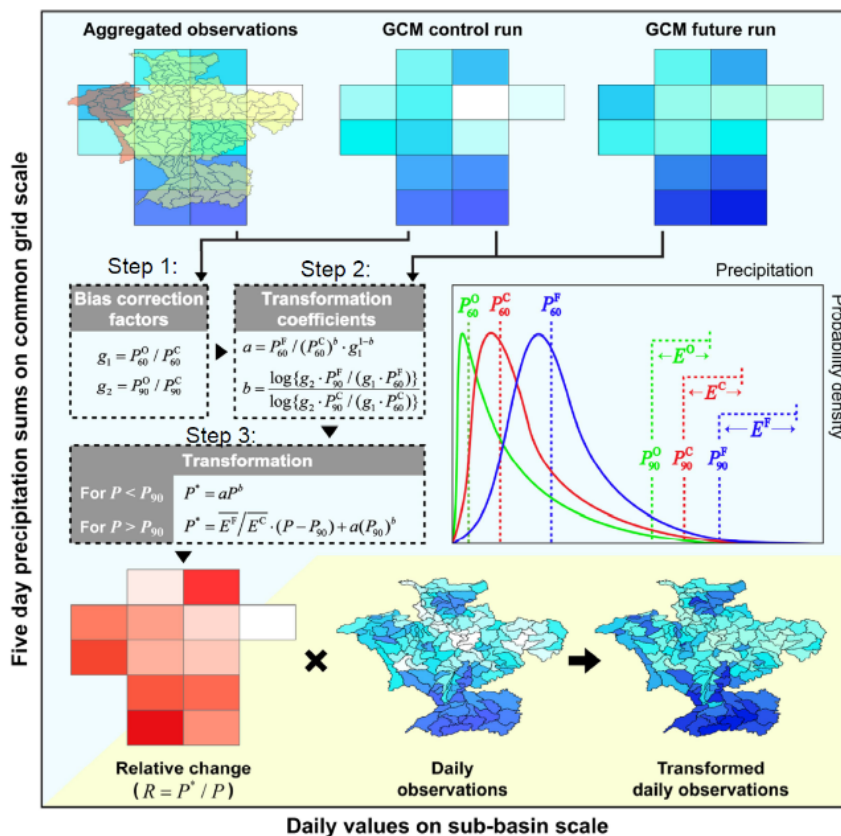


Figure 2.5: Schematic overview of the Advanced Delta-Change method (source: [18])

For the transformation of the observed 5-day precipitation sums (P) two equations are used, i.e. for precipitation sums that are smaller or larger than their 90% quantile (P_{90}). This quantile is determined per calendar month for each grid cell over the entire reference period, hence there are 12 different P_{90} values per grid cell. The transformation equations to calculate the transformed 5-day sums (P^*) make use of two transformation coefficients, i.e. a and b . These coefficients are derived from the 60% and 90% quantiles of the 5-day sum statistics. The transformation equation in the case where P exceeded the P_{90} , also uses an excess value (E). This is the part of the precipitation that exceeds the P_{90} ($E = P - P_{90}$). For the transformation equation the mean excesses for the control and future periods are used (see middle row in Figure 2.5). The coefficients a and b and the change in the mean excess vary seasonally (per calendar month) and spatially (per grid cell). Further, to derive the transformation coefficients (i.e. the ADC parameters) for each grid cell, the relevant grid cell statistics are smoothed using the 8 neighbouring grid cells (in an area of 3 x 3 cells).

The GCM control period and the observations may have somewhat different statistics. To correct for those differences a bias correction is applied. The bias correction factors are derived from the relative differences in the quantiles P_{60} and P_{90} between the GCM control simulation and the historical (reference) observations.

For the calculation of river discharges the hydrological model HBV-Rhine is used (see Section 2.4.2 for further details). In the HBV-Rhine model the Rhine basin is divided in 134 sub-basins. The final step in the ADC method is to calculate the future daily precipitation at the sub-basin scale. To achieve this, for each (common) grid cell and 5-day period a change factor R is defined. This change factor is the ratio between the transformed 5-day sum and the corresponding original 5-day sum (in the historical record aggregated observations), i.e. $R = P^* / P$ (see bottom row of Figure 2.5). The daily observations in the 134 HBV sub-basins from the historical reference period 1951-2006 are used for the final transformation. The daily precipitation in a sub-basin is multiplied by the R -value corresponding to the (common)grid cell and 5-day period. The individual days within a 5-day period are thereby transformed with an equal change factor. Consequently, a dry day within a 5-day period remain dry and the wet days are scaled with R .

Temperature transformation

In addition to the precipitation transformation also a temperature transformation is needed for hydrological modelling. The temperature transformation is the same linear transformation as in [18]:

$$T^* = \frac{\sigma^F}{\sigma^C} (T - \overline{T^O}) + \overline{T^O} + \overline{T^F} - \overline{T^C} \quad (2.1)$$

applied to the observed daily temperature T , and where T^* represents the transformed daily temperatures; $\overline{T^O}$, $\overline{T^C}$ and $\overline{T^F}$ are the calendar month mean of respectively the observed, control and future temperature; σ^C and σ^F the standard deviation of the daily control and future temperature calculated per calendar month.

The means and standard deviations are determined for each common grid cell by aggregation of the observations and bilinear interpolation of the GCM temperatures. Subsequently, the transformation is applied to daily observations for a particular sub-basin by using the common grid cell means ($\overline{T^O}$, $\overline{T^C}$, $\overline{T^F}$) and standard deviations (σ^C , σ^F) of the corresponding grid cell and calendar month.

2.3.4. KNMI Climate Scenarios

Based on GCM projections KNMI has constructed climate change scenarios specifically for the Netherlands. The so-called KNMI'06 climate scenarios were published in 2006 and were based on climate model simulations described in the IPCC Fourth Assessment Report [11]. The KNMI'06 climate scenarios [16] include two sets of four different scenarios, one set for the years around 2050 and one set for around 2100. To span a range of changes in seasonal mean temperature and precipitation in the Netherlands the scenarios are set up by a two-axis framework. One axis expresses the change in the projected global mean temperature and the other axis represents the change in the large scale atmospheric flow around The Netherlands, more specifically, the change in the strength of the western component of the atmospheric flow. These two components are selected since most of the range of changes in temperature and precipitation in The Netherlands can be related to these components. The KNMI'06 climate scenarios were constructed specifically for The Netherlands but they were also applied in the (entire) Rhine and Meuse basins to obtain discharge projections for the Rhine and Meuse rivers.

After the publication of the IPCC Fifth Assessment Report [12], the KNMI constructed new climate scenarios. These KNMI'14 climate scenarios [17] are made with the new scientific insights and climate models from the Fifth Assessment Report. The same two-axis framework as for the KNMI'06 climate scenarios was adopted, thus again with a distinction between the global mean temperature increase and the response of the regional atmospheric circulation (see Figure 2.6). The scenarios were constructed for the the periods 2016-2045, 2036-2065 and 2071-2100, respectively, '2030', '2050', and '2085'.

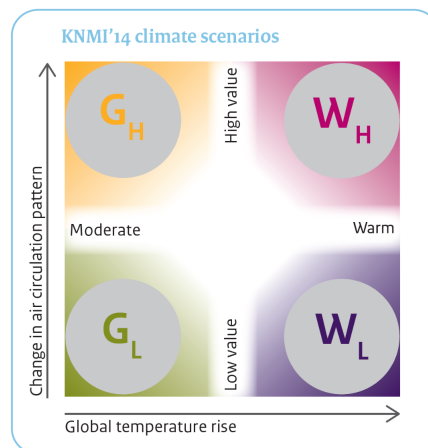


Figure 2.6: Overview of the KNMI'14 scenarios (source: [17])

The KNMI'14 climate scenarios were constructed in such a way that they span a large fraction of the spread in simulations from the Coupled Model Intercomparison Project phase 5 (CMIP5) ensemble (for further details see Section 2.3.2). For the construction of the KNMI'14 scenarios use was made of the Global Climate Model EC-Earth in combination with the Regional Climate Model RACMO2. An ensemble of 8 EC-Earth simulations driven with the RCP8.5 forcing scenario, downscaled with the RACMO2 model, was used as a basis. To construct each of the four scenarios, 5-year sub-periods were sampled from the time series of the original 8-member ensemble. Sub-periods not shorter than 5 years are used to preserve the temporal correlation structure of the original time series. The selection of the 5-yr sub-periods was based on a set of selection criteria that match the desired changes for each of the four scenarios and that, in turn, were obtained from (the spread in) the CMIP5 global climate model projections for respectively '2050' and '2085'.

The criteria for the G and W scenarios were set by the increase in global mean temperature. The G-scenarios presume a small increase (1 °C in 2050 and 1.5 °C in 2085) and the W-scenarios presume a stronger temperature increase (2 °C in 2050 and 3.5 °C in 2085). The subscript of the scenarios (L and H) is used to span the spread in precipitation change. The subscript H represent a strong response, with wetter winters and drier summers, and the subscript L represent a weak response with smaller changes in precipitation in both seasons. The selection criterium for these scenarios relates to the change in winter precipitation. For the scenarios with 'low' change in precipitation climate (G_L and W_L) a winter precipitation change of 4% per degree global warming was used. And, for the scenarios with 'high' precipitation change (G_H and W_H) a winter precipitation change of 8% per degree global warming was used. This criterium remains unchanged for '2050' and '2085'.

For the construction of the '2030' scenarios a different procedure was followed. On this short projection time scale the climate change signal is still small and this also holds for the spread between the different ensemble members. For '2030' therefore a single KNMI'14 climate change scenario was constructed. This '2030' scenario was essentially constructed as the average of the 8 EC-Earth-RACMO2 ensemble members for the period 2016-2045. A detailed description of the construction of the KNMI'14 climate scenarios is given in Lenderink et al. [20].

KNMI'14 scenarios for the Rhine basin

Consistent with the KNMI'14 scenarios for The Netherlands, KNMI'14 scenarios were constructed for the Rhine and Meuse basins as well. The aim of the KNMI'14 climate scenarios for the Rhine and Meuse basins was that they represent a considerable amount of the CMIP5 spread in the (seasonal) changes in precipitation and temperature for the Rhine and Meuse basins, as they also do for the The Netherlands. For the Rhine basin a fifth climate scenario was constructed ($W_{H,dry}$), because the most extreme KNMI'14 scenario in terms of summer drying (W_H) was not dry enough compared with the spread in the CMIP5 ensemble [19]. Nevertheless, the $W_{H,dry}$ scenario is not considered in this research, since we are primarily interested in the extreme river discharges and thus extreme precipitation events and not in extreme dry periods.

Apart from the $W_{H,dry}$ scenario, the KNMI'14 scenarios for the Rhine and Meuse basins were based on exactly the same EC-Earth-RACMO2 sampled subsets as those used for the KNMI'14 scenarios for the Netherlands. To apply the KNMI'14 climate scenarios to the hydrological model for the Rhine catchment (HBV-Rhine, see Section 2.4.2), historical precipitation and temperature time series for each of the HBV-Rhine sub-basins were transformed to the future, consistent with each of the four KNMI'14 scenarios, by making use of the ADC method (see section 2.3.3 for further details). The essence of the ADC method is that the relative changes in the extreme precipitation may be different from those in the mean precipitation. A practical advantage of this ADC method is that it also deals with the difference in spatial resolution between the HBV-Rhine catchments and the climate model grid cells [29].

2.4. Modelling from meteorology to river discharge

The series of daily precipitation and temperature of the CMIP5 simulations can be transformed into river discharges by the GRADE (Generator of Rainfall and Discharge Extremes) instrument [9]. GRADE can provide discharge series with a length of up to 50,000 years from precipitation and temperature series. For this translation the GRADE method made use of three components.

Component 1: Stochastic weather generator

The stochastic weather generators used for the Meuse and Rhine basins are based on nearest-neighbour resampling and produce very long daily rainfall and temperature series that preserve the statistical properties of the original (much shorter) series.

Component 2: Hydrological modelling

A hydrological model is used to transform the precipitation and temperature series into discharges. Within GRADE use is made of the HBV (Hydrologiska Byråns Vattenbalansavdeining) rainfall-runoff model.

Component 3: Hydrological and hydrodynamic routing

This component of GRADE routes the runoff generated by HBV through the main river. First, a simplified hydrological routing module is used in HBV, but this does not simulate well the physical processes such as retention and flooding. Therefore, a hydrodynamic routing component is added. For this purpose, the Sobek hydrodynamic model is used. However, only the largest flood waves are simulated with the Sobek model. These waves are selected from the results of the built-in routing in the hydrological model. This is done, because a full hydrodynamic simulation of the synthetic series is computationally not feasible.

2.4.1. Stochastic weather generator

The weather generator is used to generate long synthetic series of daily precipitation and temperature by using the nearest-neighbour resampling technique [1]. In the nearest-neighbour method weather variables like temperature and precipitation are sampled simultaneously with replacement from the historical data. The weather generator for the Rhine and Meuse basins do not generate rainfall at a single site, but rainfall and temperature at multiple locations simultaneously. A major advantage of resampling historical days at multiple locations simultaneously is that both the spatial association of daily rainfall over the drainage basin and the dependence of daily rainfall and temperature are preserved without making assumptions about the underlying joint distributions.

To incorporate autocorrelation resampling depends on the simulated values for the previous day. One first searches the days in the historical record that have the similar characteristics as those of the previously simulated day. Those days are the so called nearest neighbours of the previously simulated day. One of those days is selected randomly and the observed values for the day subsequent to that nearest neighbour are adopted as the simulated values for the next day.

To find the nearest neighbours a feature vector is used. The feature vector is formed out of a small number of statistics of (standardized) weather variables. The nearest neighbours are ordered using a weighted Euclidean distance. Only the k nearest ones from a certain time window are selected. This window is moving and centred on the calendar day of interest. This moving window is needed to account for the seasonal variation in the dependence between variables. One of the k nearest ones is selected randomly. But before the selection a decreasing kernel of Lall en Sharma (1996), which gives a higher weight to the closer neighbours, is used.

For the rainfall generators for the Rhine and Meuse, the weights are taken inversely proportional to the variance of the feature vector elements and k is set to 10. For the Rhine a 3-dimensional feature vector is used: the daily mean temperature in the basin, the daily mean precipitation in the basin and the daily fraction of locations with precipitation larger than 0.1 mm. For further details see Schmeits et al. [28].

The 50,000-year simulation for the Rhine made use of the historical period 1951-2008 as the base period. The 50,000-yr simulations are constructed for the reference situation [9] and for the KNMI'14 climate scenarios [29]. For the KNMI'14 climate scenario use is made of the ADC method (described in section 2.3.3) to transform the base period to the future period according the climate scenario.

2.4.2. Hydrological modelling

To transform the precipitation, temperature and potential evapotranspiration series into discharges a hydrological model is used. Within GRADE use is made of the HBV (Hydrologiska Byråns Vattenbalansavdeining) rainfall-runoff model both for the Meuse and the Rhine. HBV is a conceptual model which means that the model components represent the basin on a realistic way. A schematic overview of the HBV model is shown in Figure 2.7.

The model structure can be divided into a number of routines. In the snow routine the accumulation of snow and snow melt are determined according to the temperature. The soil routine controls which part of the rainfall and melt water forms excess water and how much is evaporated or stored in the soil. The runoff generation routine consists of an upper, non-linear reservoir representing fast runoff components and a lower, linear reservoir representing base flow.

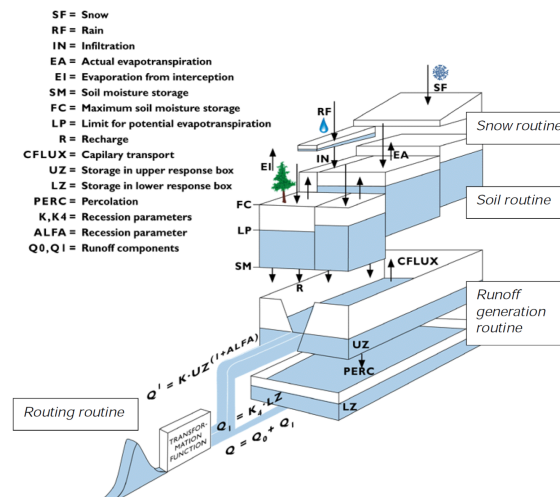


Figure 2.7: Schematic overview of the HBV rainfall-runoff model (source: [9])

To set up the HBV model the basins in the river Rhine and Meuse are subdivided into a number of sub-basins. This division is primarily done to have the same physical characteristics within a basin, and also the precipitation within a sub-basin can be considered as uniform. The Rhine basin is initially divided in 134 sub-basins. But the lakes in Switzerland have an considerable effect on the discharge. Therefore, four large lakes in Switzerland are included to the initial division of 134 sub-basins, which led to a total of 148 sub-basins [10].

The HBV model runs with a daily time step. The model input consists of daily average precipitation and temperature for each sub-basin. The model is calibrated using the GLUE (Generalized Likelihood Uncertainty Estimation) method, with the focus on high discharges.

2.4.3. Flood routing

The routing of flood waves from the various sub-basins through the main channels can be done by either the hydrological flood routing in HBV or flood routing of external hydrological or hydrodynamic models, which are fed by the simulated discharges of the HBV sub-basins.

A conceptual model as the HBV model has its limitation for flood routing, because not all the important hydrodynamic effects are included. The level of which this type of model represents the reality depends on the layout of the reservoirs in the model. For the extreme Rhine discharges in the HBV model in GRADE do not represent the real discharges well, since flooding in Germany will occur which are not included in the HBV model.

To include all the important hydrodynamic effects, such as flooding and backwater curves, an advanced hydrodynamic model is needed. The big disadvantage of using hydrodynamic routing is that the calculation requires a high computation time. Due to the computation time the hydrodynamic calculations are only done for the largest flood waves. This can be the annual maximum flood peaks or flood waves with a minimum

amount of discharge. These largest flood waves are derived from the hydrological routing results using a three-step approach:

1. First the full synthetic series (50,000 years) are simulated with the flood routing in HBV and the largest flood peaks at Lobith (or Borgharen for the Meuse) are selected.
2. Subsequently the corresponding flood waves are simulated again with the hydrodynamic routing, starting 30 days before the moment of the peak until 20 days after the moment of the peak.
3. The results of the two are combined to get a continuous discharge series.

GRADE uses a 1D SOBEK-RE model for the hydrodynamic routing. In this model flooding areas behind the dikes are included for the Upper Rhine (between Maxau and Kaub) and the Lower Rhine (between Bonn and Lobith, see figure 1.1). The potential flood areas behind the dikes are modelled as retention areas that retain water when a certain water level is reached and empties when the flood recedes. The inflow into the retention area will stop and flow along the area, when the maximum area in the retention area is reached. If the water level in the retention area exceeds a certain level, the water can outflow the area at a more downstream part of the river. So, this water will by-passes the river [10].

3

Uncertainties in future River discharges

In this chapter we want to determine the uncertainties in the future river discharges, and especially the uncertainties due to climate change. To determine these uncertainties a lot of river simulations with various climate model data and climate scenarios are required. These river simulations are available for the CMIP5 (Coupled Model Intercomparison Project phase 5) climate model simulations. Although this is a sufficient amount of climate model simulations, the river simulations were only made for a time series of 56 years. This is not sufficient to determine the uncertainties in the extreme return levels, but these simulations can be used to determine the uncertainties in the change in mean annual maximum discharge (dMHQ). In Section 3.2 the uncertainties in dMHQ are determined.

To determine the uncertainties in the return levels subsequently, use is made of a relation between dMHQ and the change in annual maximum discharge with return period T (dHQ_T). These relations are obtained with the river simulations of the KNMI'14 climate scenarios. For these climate scenarios data sets with 50,000 annual maximum discharges were constructed, which is sufficient to determine the extreme return levels. In Section 3.1 these data sets are described and the relations between dHQ_T and dMHQ for various return periods are determined.

In Figure 3.1 a flowchart is presented. This flowchart shows all the steps that are taken to determine the uncertainties in the river discharges with the available data sets (as described above). As can be seen in the flowchart, the uncertainties are first determined for the HBV (hydrological) discharges (Section 3.3). This is because the river simulations for the CMIP5 climate model data were only done with the HBV model. The uncertainties in the Sobek (hydrodynamic) discharges (Section 3.4) are determined by converting the HBV discharges in Sobek discharges with a relation between the discharges of these models (Section 3.4.1).

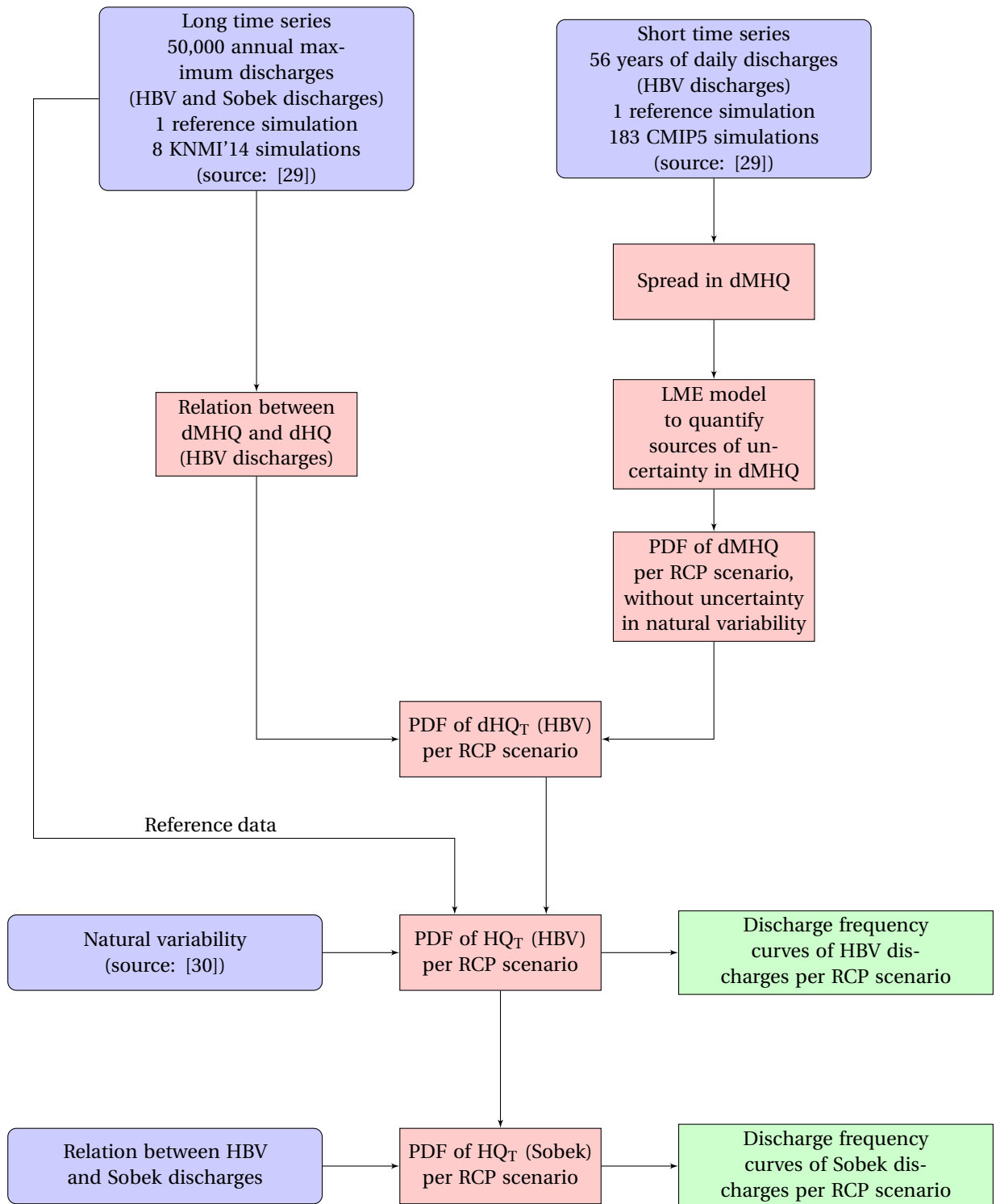


Figure 3.1: Flow chart to build the river discharge projections. Blue rectangles show the input data from external sources, the red rectangles show the progress steps and the green rectangles show the final output.

3.1. Long time series

In this research, long time series are time series consisting of 50,000 annual maximum discharges. For the river Rhine long time series were already produced for the reference situation [9] and the future situation under the KNMI'14 climate scenarios [29], using the hydrological model HBV. These long time series are used in this research to obtain a relation which can be used to assess the extreme discharges for much shorter time series. This section first describes the long time series (Section 3.1.1) and gives thereafter the obtained relation that can be used further in this research (Section 3.1.2).

3.1.1. KNMI'14 projections

The river discharge projections for the KNMI'14 climate scenarios [29] were made for the years 2050 and 2085. This is due to the fact that the KNMI'14 climate scenarios are constructed for the periods around these years. For both years a data set with 50,000 annual maximum discharges per KNMI'14 climate scenario is available. This data set is presented in Figure 3.2 as discharge frequency curves. A discharge frequency curve is a continuous representation of annual maximum discharges as a function of their return period. The return period corresponding to a certain annual maximum discharge is obtained by ranking the annual maximum discharges in the generated 50,000-year sequence in increasing order. The rank in this ordered set determines the return period.

The annual maximum discharges show rather strong random fluctuations in the upper tail of the distribution. To reduce the effect of these random fluctuations a Weissman fit is applied to the discharges with long return periods, i.e. return periods ≥ 500 years. This method makes use of the joint limiting distribution of order statistics. The Weissman fit is also used to extrapolate the annual maximum discharges beyond a return period of 50,000 years.

The KNMI'14 climate scenarios are constructed in such a way that they span a large fraction of the spread in the CMIP5 simulations in the change in precipitation and temperature. Even though these changes affect the river discharges, it is not clear if the distributions in Figure 3.2 also span the same fraction of the spread in the CMIP5 simulations. The CMIP5 simulations are needed to determine the complete spread in discharges.

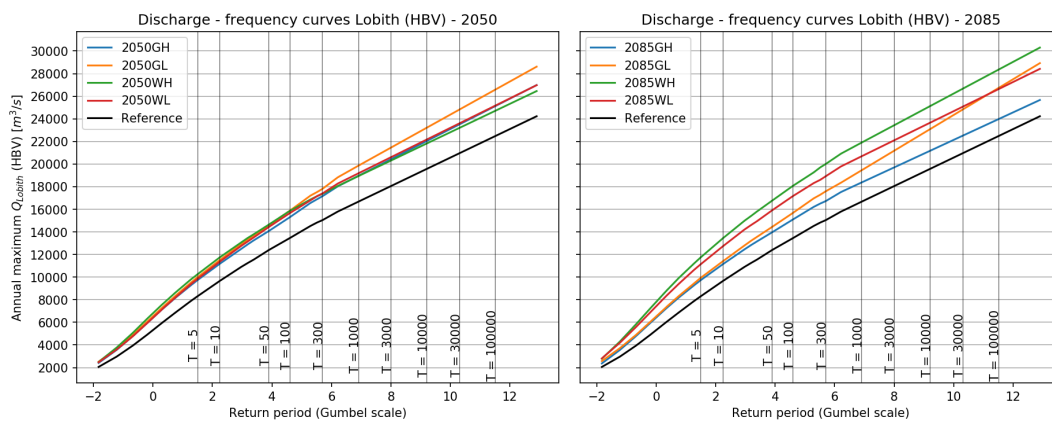


Figure 3.2: Discharge - frequency curves for the Rhine at Lobith for the KNMI'14 projections, in the left figure for the KNMI'14 scenarios around the year 2050 and in the right figure for the scenarios around the year 2085. The discharges are based on the hydrological model HBV, without the effect of upstream flooding. For the extreme discharges (return period ≥ 500 years) the data are smoothed and extrapolated by a Weissman fit. (source of the data: [29])

3.1.2. Relation dMHQ - dHQ

The changes in the annual maximum discharge for a given return period (dHQ_T) show a linear relation with the changes in mean annual maximum discharge (dMHQ). For the short time series, this relation can be used to assess the change in annual maximum discharge for any return period (so, also for the extreme river discharges) from their change in mean annual maximum discharge.

The data of the KNMI'14 projections (see Section 3.1.1) is used to determine this relation. The KNMI'14 projections for both 2050 and 2085 can be used for this, because they are all based on transformations of daily precipitation and temperature for the same reference period but with different forcings. For four return periods the data of all eight KNMI'14 projections is presented by the dots in Figure 3.3. The linear relation is obtained by a least squares fit to these dots, forced through the origin.

Figure 3.3 shows that the slope of the linear line increases with the return period. But also the error of this slope increases with the return period. Table 3.1 gives an overview of the slope and its standard error for the relations presented in Figure 3.3.

In total 35 relations were fitted for return periods ranging from 1.002 to 400,000 years. The values for intermediate return periods were obtained by linear interpolation.

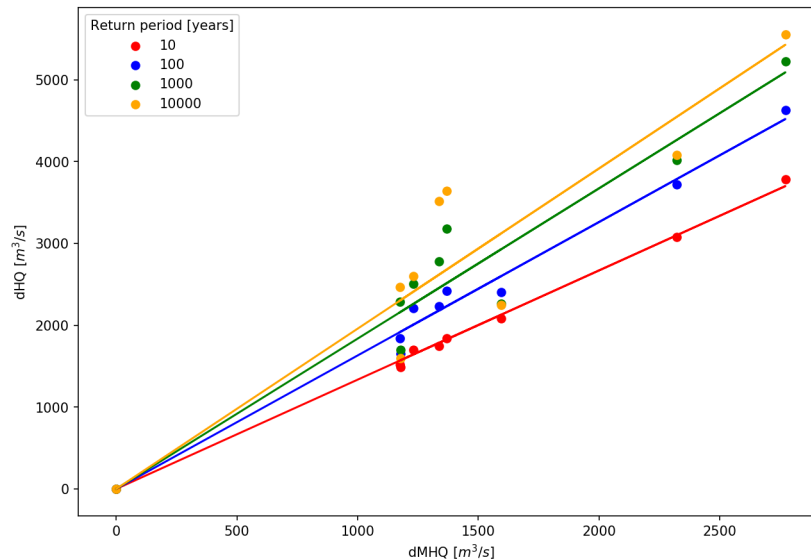


Figure 3.3: Relation between the change in mean annual maximum discharge (dMHQ) and change in annual maximum discharge (dHQ_T) for four return periods. The dots represent the data from the eight KNMI'14 projections and the linear line is the least squares fit to these dots.

Table 3.1: Overview of the slopes and standard error of the slope for the dMHQ-dHQ relations in Figure 3.3.

Return period	Slope	Std. error of the slope
10	1.33	0.0001
100	1.63	0.0013
1000	1.84	0.0087
10000	1.96	0.0210

3.2. Short time series

In this research, short time series refer to time series consisting of 56 years of daily discharges. The length of 56 years relates to the longest available historical time series with both daily precipitation and temperature data in the whole Rhine basin. This is a time series for the period 1951-2006. The daily precipitation and temperature data is used to simulate discharges with the hydrological model HBV.

The ADC-method (as mentioned in Section 2.3.3) is used to transform this historical time series of daily precipitation and temperature into future time series. The transformed time series of daily precipitation and temperature are thereafter used to simulate river discharges belonging to that specific climate. For the CMIP5 climate model simulations these transformed time series were already constructed by Sperna Weiland et al. [29].

The CMIP5 simulations consist of 183 short time series, which are used in this research to quantify the sources of uncertainty in the changes of river discharges. First the sources of uncertainty in the dMHQ will be quantified and with the relation found in Section 3.1.2 the uncertainties for any dHQ_T can be obtained.

To quantify the sources of uncertainty in dMHQ use is made of a Linear Mixed-Effects (LME) model. An LME-model is an ANOVA (Analysis of Variance) model that includes fixed effects and random effects (see [24] for details). The quantification of the sources of uncertainty with the LME-model is described in Section 3.2.1. From the LME-model a probability density function of the change in mean annual maximum discharge can be constructed, which is shown in Section 3.2.2.

3.2.1. Quantification of the sources of uncertainty

The variation in dMHQ of the 183 CMIP5 simulation runs is caused by the uncertainties in climate change projections. These uncertainties originate mainly from three sources: natural variability, model uncertainty and scenario uncertainty. The model uncertainty includes the incomplete knowledge of the physical processes governing the climate system and the technical limitations in the implementation of these processes in the climate models. The scenario uncertainty includes the uncertainty in the future forcing, comprising the future emissions of greenhouse gasses and aerosol particles and other forcing agents like land use change.

To quantify the sources of uncertainty in the ensemble of 183 simulations an LME-model is used. Mixed-effects models are primarily used to describe the relationship between a response variable and the uncertainty around this response. Here, the same approach is used as Hanel and Buishand [7] did for the sources of variation in changes of precipitation characteristics in the Rhine basin, where the response to the forcing is a fixed effect and uncertainties in the climate model response and natural variability are random effects.

Linear Mixed-Effects model

The statistical LME-model describes the variation in dMHQ as a function of the forcing, model uncertainty and natural variability. The changes in the mean annual maxima of the simulated daily discharges are based on the GCM simulations from the CMIP5 archive for a reference period (1961-1995) and a future period (2071-2100). Since the LME-model is fitted to the change in MHQ between these two periods, we consider the change in the strength of the forcing for each of the four RCP scenarios. The strength of the forcing is obtained from the estimated forcing for the two periods (as given by Meinshausen [21]). The median forcing in the reference period is 0.96 W/m^2 . After subtraction of this value from the median forcing in the future period the change in forcing becomes 1.67, 3.20, 4.08 and 6.32 W/m^2 for RCP2.6, RCP4.5, RCP6.0 and RCP8.5, respectively.

The fixed effect in the LME-model is the forcing. It is assumed that there is a linear relation between dMHQ and the forcing. Figure 3.4 gives the relation between dMHQ and the forcing. The blue dots represent the dMHQ of each GCM simulation and the red line presents the least squares fit to the mean values for each RCP. The red line shows that there is an overall increase in dMHQ with forcing ($\sim 151 \text{ m}^3/\text{s}$ per unit forcing). In addition to the overall increase, also the scatter in dMHQ increases with the forcing. Except for the RCP6.0 scenario, where the scatter is smaller. This can be explained by the fact that there are much less simulations (only 29) forced with this scenario.

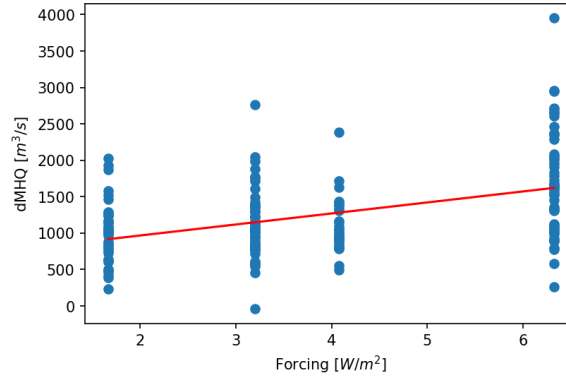


Figure 3.4: Change in mean annual maximum discharge (dMHQ) for the river Rhine at Lobith between the periods 1961-1995 and 2071-2100 as a function of the forcing for various GCM simulations. The red line represents the overall response to the forcing.

An LME-model that includes all the phenomena observed in Figure 3.4 can be described as:

$$y(i, j, k) = \alpha_0 + \alpha_1 F(j) + a_0(i) + a_1(i)F(j) + \epsilon(i, j, k) \quad (3.1)$$

where $y(i, j, k)$ represents dMHQ for simulation k of GCM i under RCP scenario j and $F(j)$ the strength of the forcing. The coefficients α_0 and α_1 are fixed constants representing the overall intercept and response to the forcing (the red line in Figure 3.4). The coefficients $a_0(i)$ and $a_1(i)$ are random variables representing the scatter around the line due to climate model uncertainty and $\epsilon(i, j, k)$ is the random error term representing natural variability. The interaction term $a_1(i)F(j)$ is needed to achieve that the scatter increases with the forcing.

The model can be interpreted as linear regression model with a random intercept $\alpha_0 + a_0(i)$ and a random slope $\alpha_1 + a_1(i)$. A standard assumption is that a_0 and a_1 are normally distributed with mean zero, variances $\sigma_{a_0}^2$ and $\sigma_{a_1}^2$ and correlation coefficient ρ_a . The random error term $\epsilon(i, j, k)$ is also assumed to be a normally distributed random variable, with mean zero and variance σ_ϵ^2 . The random errors are independent, except for the changes that are based on the same GCM simulation for the present climate. These simulations show a common natural variation during the control period, which causes a correlation ρ_ϵ . In this research it is assumed that the correlation is the same for each pair of RCPs with a common control simulation.

The random terms $a_0(i)$ and $a_1(i)F(j)$ in Equation 3.1 represent the climate model uncertainty in the sample. The effect of the Global Climate Model (GCM) on dMHQ between 1961-1995 and 2071-2100 is demonstrated in Figure 3.5. The figure gives dMHQ for the simulations grouped by GCM for RCP4.5 (left) and RCP8.5 (right). Both figures show a scatter in dMHQ within a specific GCM, this scatter is of the same order of magnitude for RCP4.5 as for RCP8.5. The scatter in dMHQ within a specific GCM can be seen as natural variability. The natural variability does not cover the total scatter in dMHQ that can be seen in Figure 3.5. There is still a scatter between the GCMs, showing the presence of a climate model effect. It is clear that this scatter is larger for RCP8.5 than for RCP4.5, indicating an interaction between the random effect and the forcing.

The LME-model in Equation 3.1 assumes that the random effect terms $a_0(i)$ and $a_1(i)F(j)$ are independent between the GCMs. This is questionable for the CMIP5 ensemble because a number of GCMs have the same driving Atmospheric Circulation Model (ACM) (see Table 2.1). When the differences between GCMs can be fully attributed to their ACM, then we have to replace GCM i by its ACM group g in Equation 3.1. A two-level LME-model is however needed for the case that the ACM only partly explains the differences between the GCMs. The two-level model contains random effects for both the GCM and the ACM group:

$$y(g, i, j, k) = \alpha_0 + \alpha_1 F(j) + a_0(g) + a_1(g)F(j) + b_0(g, i) + b_1(g, i)F(j) + \epsilon(g, i, j, k) \quad (3.2)$$

where $y(g, i, j, k)$ is the change in mean annual maximum discharge for simulation k of GCM i from ACM group g under RCP scenario j and $F(j)$ is again the strength of the forcing. The coefficients α_0 and α_1 are

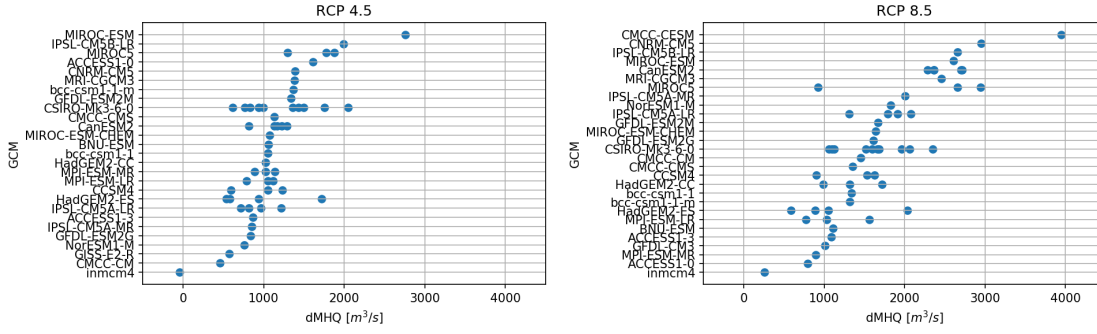


Figure 3.5: Scatter in the change in mean annual maximum discharge (dMHQ) between 1961-1995 and 2071-2100 for each GCM. In the left figure the simulations of RCP4.5 are given and in the right figure the simulations of RCP8.5. The GCMs are sorted by the value of the change or by the mean value of the change in the case of multiple runs.

fixed constants representing the overall intercept and response to the forcing (the red line in Figure 3.4). The random coefficients $a_0(g)$ and $b_0(g, i)$ represent an effect of the ACM and GCM, respectively, the random coefficients $a_1(g)$ and $b_1(g, i)$ relate to the interaction between the ACM and GCM with forcing and $\epsilon(g, i, j, k)$ is a random error term representing natural variability.

The random coefficients $a_0(g)$, $a_1(g)$, $b_0(g, i)$ and $b_1(g, i)$ are assumed to be normally distributed with mean zero, variances $\sigma_{a_0}^2$, $\sigma_{a_1}^2$, $\sigma_{b_0}^2$ and $\sigma_{b_1}^2$, and correlation ρ_a (for a_0 and a_1) and ρ_b (for b_0 and b_1). The random error term $\epsilon(g, i, j, k)$ is also assumed to be normally distributed with mean zero and variance σ_ϵ^2 . It is further assumed that each of the variables $a_0(g)$, $a_1(g)$, $b_0(g, i)$ and $b_1(g, i)$ are independent for different g and i and that the level-2 random effects are independent of the level-1 random effects.

In this study 11 different statistical models are assessed (see Table 3.2 for an overview). These models describe the processes and effects mentioned above. The models have fixed coefficients only (called m_0 and m_1), single-level mixed effects considering grouping on atmospheric models (m_2 to m_4) or global climate models (m_5 to m_7) or the two-level mixed effects (m_8 to m_{10}). Some models only include random intercept terms (m_2 , m_5 and m_8), or only the random interaction with forcing (m_3 , m_6 and m_9), while other models include both (m_4 , m_7 and m_{10}). The model parameters are estimated with the maximum likelihood method (see Pinheiro and Bates [24] for further details).

Table 3.2: Overview of statistical models

Model	Type	Fixed effect	Level-1 random effect	Level-2 random effect	Random error
m_0	Fixed	α_0			$\epsilon(i, j, k)$
m_1	Fixed	$\alpha_0 + \alpha_1 F(j)$			$\epsilon(i, j, k)$
m_2	Mixed	$\alpha_0 + \alpha_1 F(j)$	$a_0(g)$		$\epsilon(g, j, k)$
m_3	Mixed	$\alpha_0 + \alpha_1 F(j)$	$a_1(g)F(j)$		$\epsilon(g, j, k)$
m_4	Mixed	$\alpha_0 + \alpha_1 F(j)$	$a_0(g) + a_1(g)F(j)$		$\epsilon(g, j, k)$
m_5	Mixed	$\alpha_0 + \alpha_1 F(j)$	$a_0(i)$		$\epsilon(i, j, k)$
m_6	Mixed	$\alpha_0 + \alpha_1 F(j)$	$a_1(i)F(j)$		$\epsilon(i, j, k)$
m_7	Mixed	$\alpha_0 + \alpha_1 F(j)$	$a_0(i) + a_1(i)F(j)$		$\epsilon(i, j, k)$
m_8	Two-level	$\alpha_0 + \alpha_1 F(j)$	$a_0(g)$	$b_0(g, i)$	$\epsilon(g, i, j, k)$
m_9	Two-level	$\alpha_0 + \alpha_1 F(j)$	$a_1(g)F(j)$	$b_1(g, i)F(j)$	$\epsilon(g, i, j, k)$
m_{10}	Two-level	$\alpha_0 + \alpha_1 F(j)$	$a_0(g) + a_1(g)F(j)$	$b_0(g, i) + b_1(g, i)F(j)$	$\epsilon(g, i, j, k)$

Model selection

The selection of the statistical model is based on three criteria; the Akaike information criterion (AIC), a lack-of-fit statistic and QQ-plots. The AIC gives the model that best fits of the selected models, the lack-of-fit statistic and the QQ-plots tell something about the adequacy of the fit. The QQ-plots show if the assumption of normally distributed coefficients is correct.

The Akaike information criterion (AIC) is defined as $AIC = -2\ln(L) + 2q$, where $\ln(L)$ is the log likelihood and q is the number of unknown parameters. A good fit results in a large value for the likelihood and thus a small $-2\ln(L)$. The term $2q$ can be thought of as a penalty for heavily parameterized models. The statistical model with the lowest AIC is selected, as this is the model that fits best. In Table 3.3 the AIC values of all the 11 statistical models are given. The lowest value of AIC is found for the single-level model with a random effect by GCM and without random intercept (model m_6). For the models with a random intercept and slope (m_4 , m_7 and m_{10}), the AIC is also given for the case where the correlation parameters ρ_a and ρ_b are set to zero. This results in lower values of AIC. In Table 3.3 these models are presented with italicized text. The AIC of model m_7 , without the correlation parameter, is very close to the lowest AIC. Model m_7 is comparable with model m_6 , it only has the random intercept as an additional parameter. Both models could be considered.

The lack-of-fit statistic compares the estimate of σ_ϵ^2 from the LME-model with a model-free estimate of the variance due to natural variability (s_{nvar}^2). This model-free estimate is obtained from the multiple runs of the same GCM under the same forcing scenario in the CMIP5 data. The sum of squares within these model runs is given by

$$SS_{nvar} = \sum_{ijk} [y(i, j, k) - \bar{y}(i, j, \cdot)]^2 \quad (3.3)$$

where $\bar{y}(i, j, \cdot)$ is the average change in mean annual maximum discharge of all the available runs of GCM i for forcing scenario j . The GCMs for which there is only one run available for the forcing scenario do not contribute to SS_{nvar} . The model-free estimate is given by

$$s_{nvar}^2 = SS_{nvar} / df_{nvar} \quad (3.4)$$

where df_{nvar} is the associated degrees of freedom:

$$df_{nvar} = \sum_{ij} n_{run}(i, j) - \sum_j n_{GCM}(j) \quad (3.5)$$

with $n_{run}(i, j)$ the number of available runs for GCM i under forcing scenario j and $n_{GCM}(j)$ the number of distinct GCMs for forcing scenario j . The values of the lack-of-fit statistic for each model are given in Table 3.3. A ratio of 1.00 means that there is no lack-of-fit, the closer to 1.00 the better the fit is. Following the AIC the best LME models are model m_6 and model m_7 , with an almost equal value for the AIC. The lack-of-fit statistic show a better result for model m_7 , without the correlation parameter. The value of the lack-of-fit statistic for model m_6 is still relatively low compared to the values for most other models.

The random coefficients in the models are assumed to be normally distributed. This assumption is verified by quantile-quantile (QQ) plots. In these plots the estimated random coefficients for each GCM and the residuals are divided by their standard deviation and then compared with the quantiles of the standard normal distribution. For dMHQ the QQ plots are shown in Figure 3.6 for model m_6 (left panel) and model m_7 without the correlation parameter (right panel). The top and middle row give the QQ plots of the random coefficients; the random intercept $a_0(i)$ and the random slope $a_1(i)$. The bottom row gives the QQ plots for the residuals ϵ . For both models the random slope and residuals do not indicate any substantial deviation from the assumed normal distribution. The deviations are for model m_6 slightly smaller than for model m_7 . The QQ plot for the random intercept of model m_7 , however, indicates a substantial deviation from the assumed normal distribution, indicating that this model may not be correct.

The results of model m_6 and model m_7 are very similar, they both fit the data quite well. However, the assumption of normally distributed random coefficients is for model m_6 better than for model m_7 . The AIC shows a slightly better fit for model m_6 than for model m_7 . But the lack-of-fit test gives a better result for model m_7 than for model m_6 . Overall it looks like model m_6 is the slightly better model. This model is also the most simple model, since it has one coefficient less. Therefore, it is chosen to use model m_6 .

Table 3.3: Number of parameters (q), the Akaike information criterion (AIC) and the lack-of-fit statistic ($\sigma_\epsilon^2/s_{nvar}^2$) for each statistical model. The model that fitted with the lowest AIC value is printed in bold. For the models indicated with italic font the correlation (ρ_a , ρ_b) between random intercepts and slopes is set to zero.

Model	q	AIC	$\sigma_\epsilon^2/s_{nvar}^2$
m_0^*	2	2862.222	2.48
m_1^*	3	2822.915	1.99
m_2	5	2778.724	1.66
m_3	5	2768.878	1.64
m_4	6	2770.618	1.48
m_4	7	2772.982	1.48
m_5	5	2773.195	1.22
m_6	5	2757.328	1.19
m_7	6	2757.972	1.10
m_7	7	2759.639	1.10
m_8	6	2775.205	1.22
m_9	6	2759.306	1.23
m_{10}	8	2759.941	1.08
m_{10}	10	2763.738	1.10

* For models m_0 and m_1 parameters are based on an ordinary least squares fit, assuming complete independence of the $\epsilon(i, j, k)$'s.

Model parameters

Model m_6 is selected as the best model. This model is a single-level mixed effects model with an interaction between a random climate model effect and the forcing. The parameters of the model are the fixed coefficients α_0 and α_1 , the random slope $a_1(i)$, the random error term $\epsilon(i, j, k)$ and the correlation in the random error term ρ_ϵ for the changes that are based on the same GCM simulations for the present climate. The random slope and random error term are assumed to be normally distributed, with mean zero and variances $\sigma_{a_1}^2$ and σ_ϵ^2 . So, for model m_6 an estimation is made for the parameters α_0 , α_1 , $\sigma_{a_1}^2$, σ_ϵ^2 and ρ_ϵ .

The estimated values of the parameters are shown in Table 3.4. The table gives the lower and upper bound of the 95% confidence interval as well. This is an interval which contains the true parameter with a probability of 95%.

Table 3.4: Overview of the model parameters for statistical model m_6 . For each parameter the estimated value and the lower and upper bound of the 95% confidence interval are given.

Parameter		Estimated value	Lower bound	Upper bound
α_0	[m ³ /s]	676.20	538.92	813.48
α_1	[m ³ /s per W/m ²]	150.69	102.87	198.52
σ_{a_1}	[m ³ /s per W/m ²]	99.55	69.00	143.63
σ_ϵ	[m ³ /s]	413.61	363.45	470.70
ρ_ϵ	[-]	0.348	0.198	0.495

For the uncertainty analysis the uncertainty in α_0 , α_1 and σ_{a_1} is considered. To include this uncertainty a probability distribution for each of these parameters is needed. For the fixed coefficients α_0 and α_1 the 95% confidence interval assumes that their point estimates are normally distributed. The mean and standard deviation of the underlying normal distribution can be obtained as:

$$\mu = [\text{upper bound} + \text{lower bound}]/2.0 \quad (3.6)$$

$$\sigma = [\text{upper bound} - \text{lower bound}]/3.92 \quad (3.7)$$

The standard deviation of the random slope σ_{a_1} is not normally distributed. The confidence interval in Table

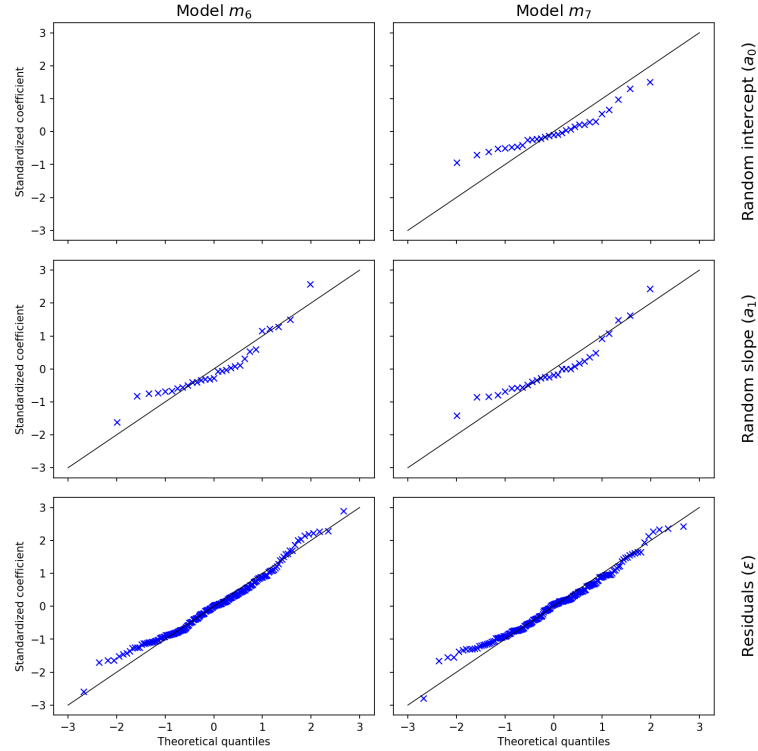


Figure 3.6: Quantile-quantile (QQ) plots for model m_6 (left) and model m_7 (right). The QQ plots verify if the assumption of normally distributed coefficients of the models is correct. The QQ plots of the random intercept $a_0(i)$ (top), the random slope $a_1(i)$ (middle) and residuals $\epsilon(i, j, k)$ (bottom) are given. Note that there is no random intercept in model m_6 .

3.4 assumes a log-normal distribution. The two parameters μ and σ of the log-normal distribution, i.e. the mean and standard deviation of the logarithm of σ_{a_1} can be found by:

$$\mu = [\ln(\text{upper bound}) + \ln(\text{lower bound})]/2.0 \quad (3.8)$$

$$\sigma = [\ln(\text{upper bound}) - \ln(\text{lower bound})]/3.92 \quad (3.9)$$

The probability distributions of the parameters that are included in the uncertainty analysis are given in Table 3.5. The uncertainty analysis also requires the correlation ρ between the estimates of the fixed coefficients α_0 and α_1 . The maximum likelihood estimate of ρ equals -0.481. The estimated fixed effect part of the LME-model is a linear combination of two normally distributed estimates, which has also a normal distribution. This distribution has mean $\mu_{\alpha_0} + \mu_{\alpha_1} F(j)$ and standard deviation $\sqrt{[\sigma_{\alpha_0}^2 + F(j)^2 \sigma_{\alpha_1}^2 + 2\rho \sigma_{\alpha_0} \sigma_{\alpha_1} F(j)]}$

Table 3.5: Overview of the probability distributions of the parameters of statistical model m_6 that are included in the uncertainty analysis. For each parameter the μ and σ of the distribution is given.

Parameter	Distribution	μ	σ
α_0	Normal	676.20	70.04
α_1	Normal	150.69	24.34
σ_{a_1}	Log-normal	4.60	0.187

3.2.2. Change in mean annual maximum discharge

The LME-model describes the change in mean annual maximum discharge (dMHQ) in simulations for the river Rhine at Lobith between the periods 1961-1995 and 2071-2100 as function of the forcing, including its uncertainty. These simulations were made with the hydrological model HBV, which means that the effect of upstream flooding is not included in these discharge simulations.

For a particular forcing a PDF (Probability Density Function) of dMHQ can be constructed by taking a large number of random draws from the LME-model and the distributions of its parameters. This can be done for any forcing, but in this research we stick to the four RCP forcings for 2085. Further in this research, the natural variability component in the LME-model is not included in the simulated PDF. This component refers to the possible differences in mean annual maximum discharges resulting from random fluctuations. For the uncertainty analysis of the annual maximum discharges, the influence of natural variability on the estimated return level from the GRADE-instrument is, however, of interest. This influence increases with return period (see Boogaard et al. [30]). The influence of natural variability on the return levels of the annual maximum discharge is added in a later stage (together with the influence of the uncertainty in the HBV parameters, see Section 3.3.1).

The PDFs of dMHQ per RCP are given in Figure 3.7. As already mentioned above, these PDFs only include the climate model uncertainty and parameter uncertainty in the LME-model. From the figure it can be seen that the mean and standard deviation of the dMHQ increase with the forcing.

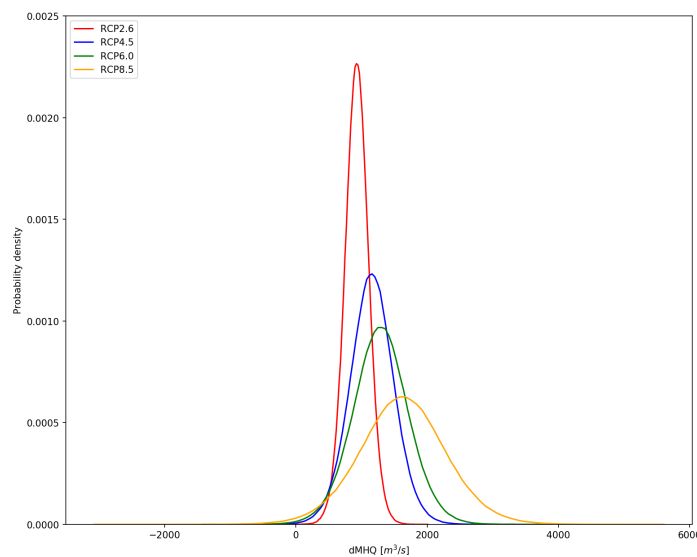


Figure 3.7: Probability density functions of the change in mean annual maximum discharge (dMHQ) between the periods 1961-1995 and 2071-2100 for the river Rhine at Lobith. The discharges are based on the hydrological model HBV. The PDF is given per RCP scenario, and includes climate model uncertainty and the uncertainty in the LME-parameters. The natural variability is not yet included.

3.3. HBV discharge projections

Within the GRADE-instrument the hydrological model HBV is used to transform the daily precipitation and temperature series into daily river discharges for the river Rhine at Lobith (see Section 2.4 for further details). The river discharges in the short time series (Section 3.2) are only simulated with the HBV model and therefore the analysis of dMHQ (section 3.2.2) was also based on HBV discharges. This analysis forms the basis for the determination of the uncertainties in annual maximum discharge per return period (HQ_T). In this section HQ_T is determined for the HBV discharges.

3.3.1. Annual maximum discharge

The return levels of annual maximum discharge (HQ_T) at Lobith are used for flood risk assessment projects along the Rhine in The Netherlands. Therefore, the uncertainties in HQ_T are of great interest for dike design considerations. As already mentioned above, the analysis of dMHQ is used to determine the uncertainties in HQ_T . In the flowchart of Figure 3.8 the steps are given, which are taken to obtain HQ_T . These steps can be taken for any return period to get the PDF of the HQ_T with that return period.

In the fourth step samples are taken from a normal distribution that includes the natural variability and HBV uncertainties. The standard deviation of this distribution is determined by Van den Boogaard et al. [30]. This study shows that the natural variability and HBV uncertainties increase with the return period, and therefore the standard deviation is given per return period. The phenomenon of an increasing natural variability is not treated well when natural variability is added in the PDF of dMHQ. Therefore, the natural variability term was ignored in the PDF of dMHQ and the standard deviations found by Van den Boogaard et al. [30] are used here for the HQ_T instead.

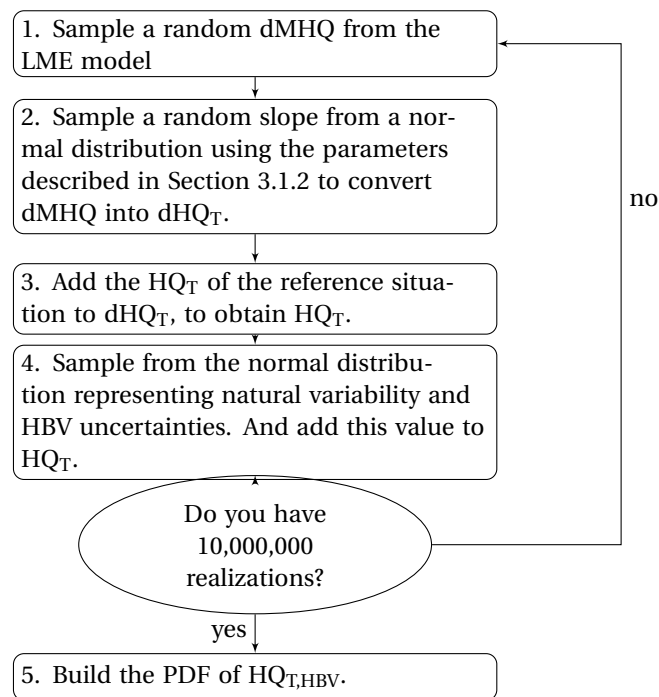


Figure 3.8: Flowchart to determine the distribution of $HQ_{T,HBV}$ for a given return period.

As the flowchart shows, with 10,000,000 samples a PDF of the HQ_T is built. In Figure 3.9 the PDFs for four return periods and the four RCPs are given. These PDFs include the climate model uncertainties, regression uncertainties, HBV uncertainties and natural variability. From the figure it can be seen that all distributions are very close to a normal distribution. The mean and standard deviation increase with the return period. For a specific return period the mean and standard deviation also increase with the forcing of the RCP, these differences are, however, much smaller than those between the return periods.

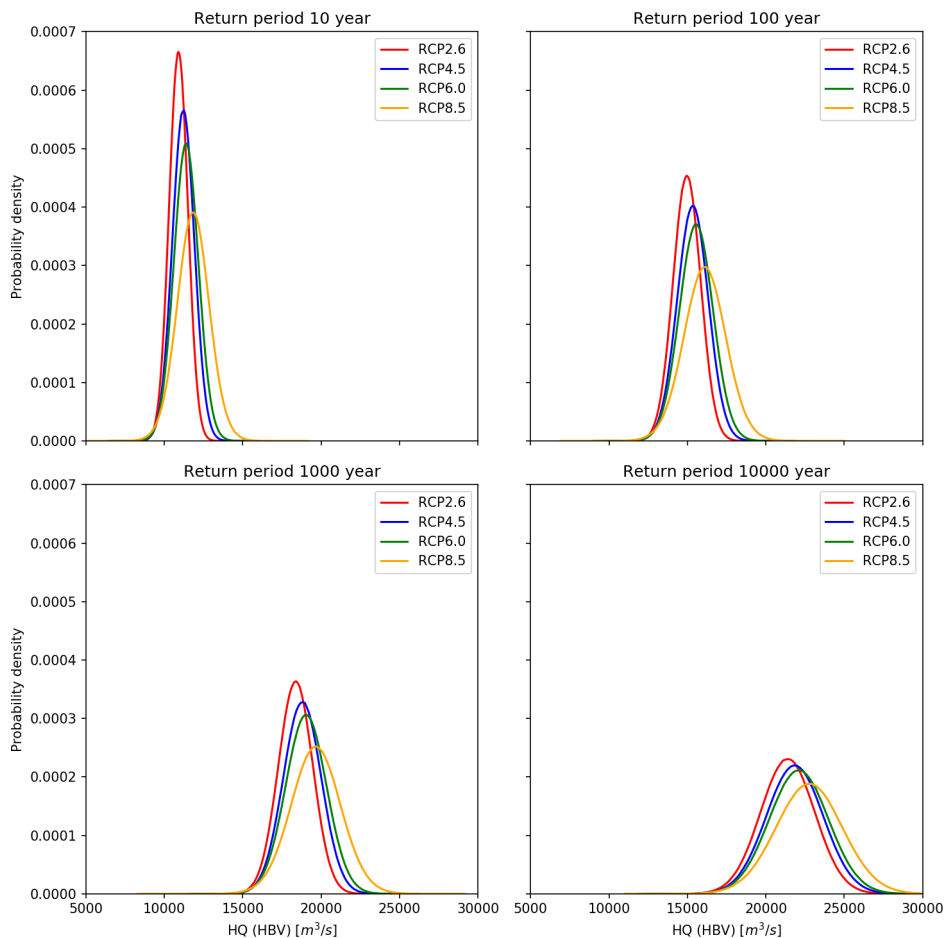


Figure 3.9: Probability density function (PDF) of the T-year return level of the annual maximum discharge (HQ_T) for the Rhine at Lobith in 2085. The PDFs are given for the four RCPs and return periods of 10 years (upper left), 100 years (upper right), 1000 years (lower left) and 10000 years (lower right). The discharges are simulated with the hydrological model HBV, upstream flooding is therefore not included. The PDFs include the uncertainty in climate model, LME-model parameters, slope of the regression, HBV model and natural variability.

3.3.2. HBV discharge frequency curves

To represent the various distributions of the return levels a discharge frequency curve can be used. In Figure 3.10 the discharge frequency curves for the four RCPs and the reference situation are presented. The reference situation is represented by the black line and the grey area represents a 95% confidence region for HQ. This confidence region only includes the HBV uncertainties and natural variability (as described in Van den Boogaard et al. [30]). The return levels for the various RCPs are given by the coloured lines, with the continuous lines representing the medians of the distributions and the dashed lines the upper and lower bounds of the 95% confidence intervals. These confidence intervals include all uncertainties described earlier.

The discharge frequency curves in Figure 3.10 show that the median and the width of the confidence interval increase with the return period and with the forcing (which already could be seen from the PDFs in the previous section). It is furthermore notable that the differences between the RCPs are small compared

with the widths of the confidence intervals for HQ_T . The confidence interval is already wide in the reference situation, which indicates that the natural variability and HBV uncertainties are the main source of the total uncertainty.

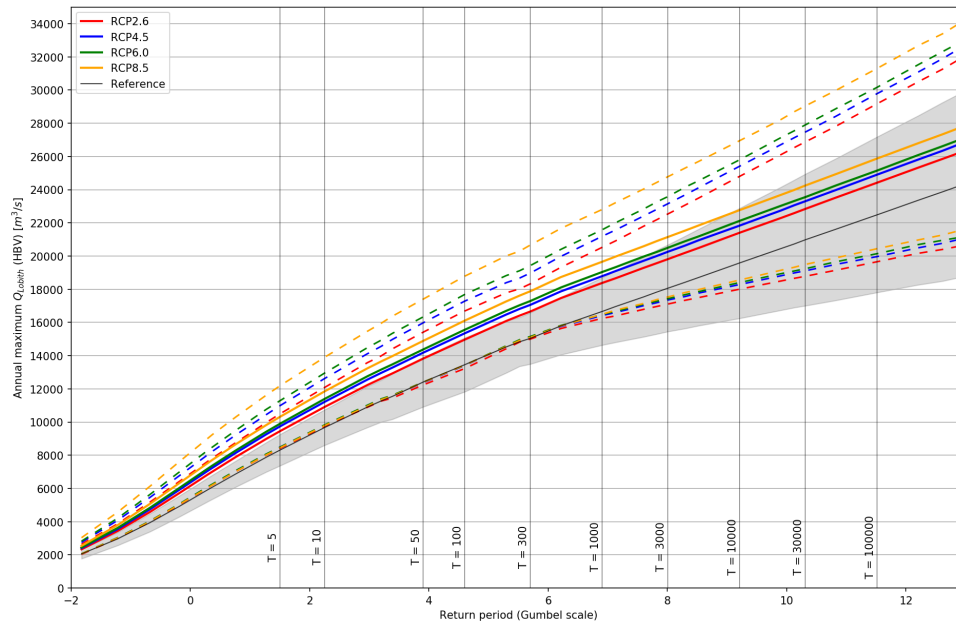


Figure 3.10: HBV discharge frequency curves for the Rhine at Lobith in 2085. The discharges are simulated with the hydrological model HBV, without the effect of upstream flooding. The grey area around the reference (black line) represents a 95% confidence region. The dashed lines give the upper and lower bounds of the 95% confidence interval for HQ_T for each RCP.

Table 3.6: Overview of the discharge extremes presented in Figure 3.10 for a number of return periods in 2085.

Return period [years]	Reference		RCP2.6		RCP4.5		RCP6.0		RCP8.5	
	Median [m ³ /s]	Width Cfd. Int. [m ³ /s]	Median [m ³ /s]	Width Cfd. Int. [m ³ /s]	Median [m ³ /s]	Width Cfd. Int. [m ³ /s]	Median [m ³ /s]	Width Cfd. Int. [m ³ /s]	Median [m ³ /s]	Width Cfd. Int. [m ³ /s]
10	9669	2148	10907	2353	11215	2788	11391	3119	11842	4114
50	12404	2983	13816	3176	14168	3607	14369	3944	14884	4989
100	13452	3247	14965	3450	15340	3907	15556	4261	16108	5374
300	15042	3086	16659	3333	17062	3864	17293	4274	17881	5530
1000	16673	4095	18375	4303	18799	4769	19043	5143	19663	6324
3000	18058	5249	19815	5420	20253	5823	20503	6149	21143	7227
10000	19577	6629	21392	6774	21844	7120	22104	7408	22764	8376
30000	20962	7938	22832	8069	23296	8382	23564	8639	24244	9534
100000	22481	9402	24408	9522	24889	9805	25165	10037	25866	10859

3.4. Sobek discharge projections

The discharge projections in Section 3.3 are based on the discharges simulated with the hydrological model HBV. This hydrological model does not include all the important hydrodynamic effects, such as backwater effects and upstream flooding. In the GRADE instrument the hydrodynamic model Sobek is used to simulate the annual maximum discharges with these effects. In this research, the Sobek discharges are obtained from the HBV discharges and the relation between HBV and Sobek discharges. This relation is obtained from earlier discharge simulations with Sobek (simulations with the KNMI'06 or KNMI'14 climate scenarios).

The steps taken to obtain the distribution of the HQ_T based on Sobek discharges are given in the flowchart in Figure 3.11. This flowchart does not differ much from the one for the HBV discharges (Figure 3.8), just two extra steps are needed. The first extra step is to transform the HBV (hydrological) discharge in a Sobek (hydrodynamic) discharge with a relation between the quantiles of the discharges of these two models, this step is further described in Section 3.4.1. The other step is to add the additional uncertainties caused by the Sobek model, this step is further described in Section 3.4.2.

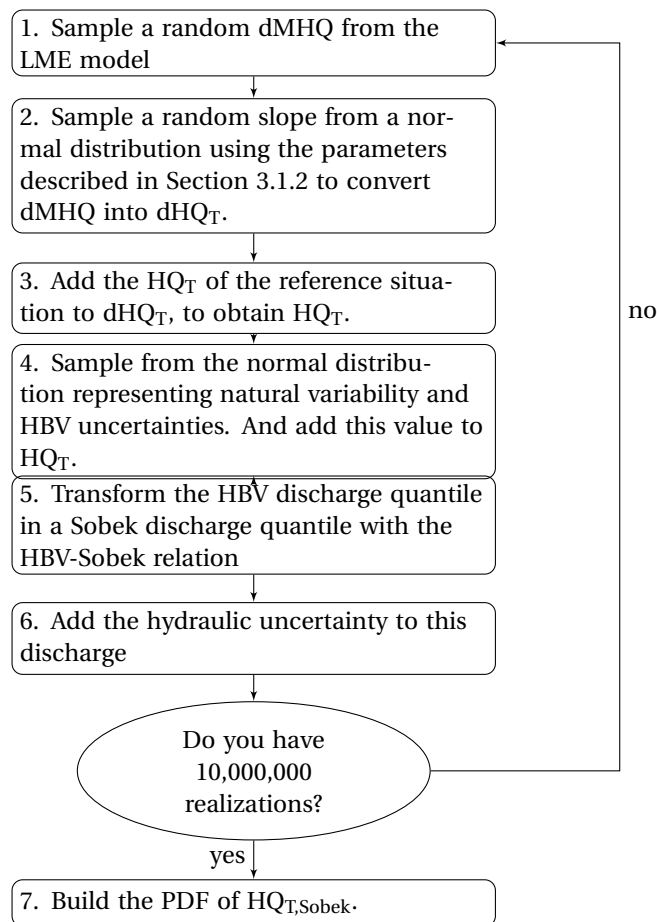


Figure 3.11: Flowchart to determine the distribution of $HQ_{T,Sobek}$ for a given return period.

3.4.1. HBV-Sobek relation

As shown in the flowchart of Figure 3.11 the Sobek (hydrodynamic) discharges are obtained by a regression on the HBV (hydrological) discharges. For this regression a data set with both the Sobek and HBV discharges is required. Such data sets are available for the reference situation, the KNMI'06 scenarios and the KNMI'14 scenarios.

The Sobek discharges in the Grade instrument are only simulated for the flood waves containing the annual maximum discharges simulated with the HBV model. For the reference situation and the KNMI'06 scenarios all these flood waves are simulated. For the KNMI'14 scenarios Sobek discharges are only simulated when the annual maximum discharges of the HBV model are larger than 10,000 m³/s. This saves a lot of time and for discharges below 10,000 m³/s the differences between the HBV and Sobek discharges are small.

The datasets of the reference situation, the KNMI'06 scenarios and the KNMI'14 scenarios can all be used to obtain the relation between HBV and Sobek discharges. A disadvantage of the data set of the reference situation is the limited amount of extreme discharges ($Q_{HBV} > 18000$ m³/s), which makes this part of the relation more uncertain.

The KNMI'06 and KNMI'14 scenarios have more extreme discharges and are therefore more useful. The dike design guideline in The Netherlands (Ontwerpinstrumentarium 2014 (OI2014)) made for the relation between HBV and Sobek discharges use of the KNMI'06 2100 W+ scenario. The 2100 W+ scenario is the KNMI'06 scenario with the largest increase in extreme discharges at Lobith. Hegnauer [8] fitted a non-linear relation to the regular (HBV, Sobek) points. Although there is a clear relation between the HBV and Sobek discharges, there is also a lot of scatter around the fitted line. This may lead to an underestimation of large return levels of the Sobek discharges. The main difficulty of the use of this relation in our study is that we have only a sample of return levels of the HBV discharges rather than the regular HBV discharges.

In order to obtain a suitable relation to convert the return levels of the HBV discharges into return levels of the Sobek discharges we regressed the quantiles of the Sobek discharges on the quantiles of the HBV discharges. For this purpose the highest HBV discharge of the data set is plotted against the highest Sobek discharge of the same data set, the second highest HBV discharge against the second highest Sobek discharge, and so on. Figure 3.12 shows the ordered data points of the KNMI'06 2100 W+ scenario. The black line is the least squares fit to these points. For this line it is decided to use the same type of regression line as Hegnauer did for his regression line. The regression line in Figure 3.12 is described by:

$$Q_{Sobek} = \alpha_1 + \alpha_2 \cdot (Q_{HBV} - \alpha_3) + \alpha_4 \cdot \ln(1 + \exp(\alpha_5 \cdot (Q_{HBV} - \alpha_3))) \quad (3.10)$$

where:

$$\alpha_1 = 12895, \quad \alpha_2 = 0.911, \quad \alpha_3 = 13752, \quad \alpha_4 = -160.33, \quad \alpha_5 = 2.8 \cdot 10^{-3} \quad (3.11)$$

The uncertainty of the parameters in Eq. 3.10 is not considered in this study. The robustness of this relation to climate change is also not explored.

The regression line can also be based on the data set of one of the KNMI'14 scenarios. The KNMI'14 scenarios show however a somewhat different relation between the quantiles of the HBV and Sobek discharges than the KNMI'06 scenarios (see Figure 5.1). In Section 5.1 the behaviour of the KNMI'14 scenarios is further discussed. It seems that the KNMI'06 2100W+ scenario is more plausible than the KNMI'14 2085WH, but we also want to stay as close as possible to the OI2014. Therefore, the regression used in this research is done with the relation of the discharge quantiles of the KNMI'06 2100 W+ as given by Equation 3.10.

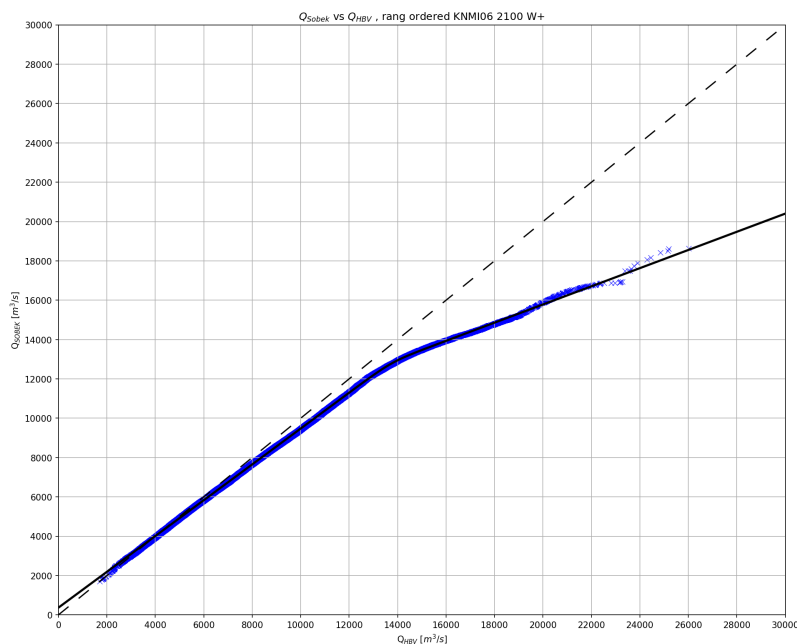


Figure 3.12: Relation between the discharges from the hydrological model HBV and the hydraulic model Sobek. Based on the ordered data of the KNMI'06 2100 W+ projection.

3.4.2. Hydraulic uncertainty

The last uncertainty that needs to be determined is the hydraulic uncertainty in the Sobek model. This uncertainty includes the uncertainties in the process of flooding in the Sobek model, consisting of 1) whether emergency flood protection measures are taken or not; 2) the actual height of the dikes; 3) the volume of the retention areas behind the dikes; 4) the failure or non-failure of the dikes after overtopping; and 5) the bottom friction. In Prinsen et al. [25] for each of these sources, an estimate is made for the range and probability distribution of the corresponding Sobek parameter values.

It is common that emergency measures are taken into account during high water levels in the Rhine. For the discharge arriving in The Netherlands it is important to take these emergency measures into account, since less dikes will fail and ultimately more water will flow to The Netherlands. There are no guidelines that describe the height and location of the emergency flood protection measures, and therefore these measures are a large source of uncertainty. Examples in the past show that in a short period a lot of sand bags can be placed. What will happen in reality is very uncertain, it is assumed that the extra dike height will be in the range of 0 to 0.5 meter.

The height of the dikes is determined with very accurate measurement systems, but the measured height is still uncertain. The real dike height varies with ± 0.10 meter from the measured dike height. The volume of the retention area behind the dikes is important for the storage of the flooded water. The water that flows into the retention area is delayed before it flows further downstream. Until the retention area is full the flood wave will be damped, and when the retention area is full all the upstream water will flow downstream. The volume of the retention areas is determined by height models, but these models do not include all elements (such as obstacles) in the retention area which causes uncertainty in the total volume of the area. A realistic assumption is that the volume of the retention area can vary in a range of $\pm 20\%$ around its theoretical volume.

The bottom friction is hard to determine. It cannot be measured directly and varies in time, with location and discharge level. Experts estimated the values of the bottom friction, these values can vary in a range of $\pm 20\%$ around the chosen value.

The last source of uncertainty is the failure or non-failure of the dike after overtopping. It is assumed that the dikes won't fail until the water flows over the dike. After overtopping a breach in the dike will grow, but

not in all cases. In Paarlberg [23] the effects of failure or non-failure of the dikes is described. He concludes that there is no significant difference in the discharge at Lobith if the upstream dike will fail or not after overtopping.

In Prinsen et al. [25] the discharge frequency curve of the Rhine discharge at Lobith is determined. Including the hydraulic uncertainty leads to higher discharge return levels, see Figure 3.13. In Hegnauer et al. [9] the discharge frequency curve without the hydraulic uncertainty is determined. Not only the mean return level of the discharge is higher, but also the width of the confidence interval is larger in the case where the hydraulic uncertainty is included.

The increase in discharge return level can be explained by the fact that most of the processes that are included for the hydraulic uncertainty do increase the discharge return level. Especially the emergency flood protection do have a large impact on the increase of the discharge return level. The larger width of the confidence interval is the logical consequence of adding extra sources of uncertainty.

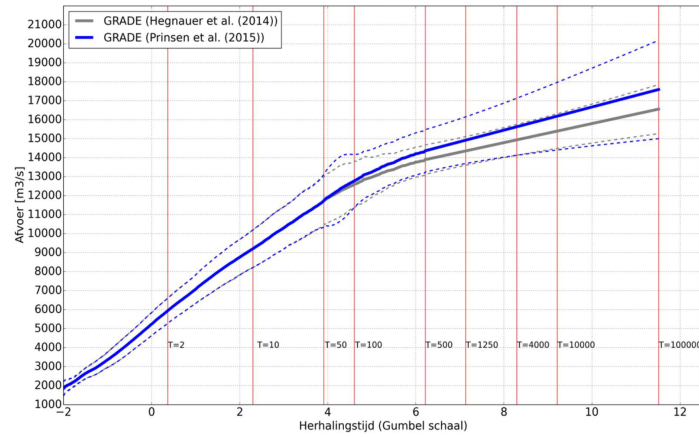


Figure 3.13: Discharge frequency curves for the Rhine at Lobith for the present climate and the situation without hydraulic uncertainty (Hegnauer et al. [9]) and the hydraulic uncertainty included (Prinsen et al. [25]) For both discharge frequency curves 95% confidence bands are given. (source: [25])

To include the hydraulic uncertainty found in Prinsen et al. [25] an equation is formulated:

$$Q^+ = Q^- + \Delta Q \quad (3.12)$$

where:

Q^- is the discharge return level at Lobith calculated in GRADE with Sobek, without the hydraulic uncertainty.

Q^+ is the discharge return level at Lobith where the hydraulic uncertainty is included.

ΔQ is the Q^- depended addition to the discharge return level as a result of the hydraulic uncertainty.

For ΔQ the following equation is found:

$$\begin{aligned} \Delta Q &= 0 \quad \text{for } Q^- < Q_0 \\ \Delta Q &= \alpha \cdot (Q^- - Q_0) \quad \text{for } Q^- \geq Q_0 \end{aligned} \quad (3.13)$$

where:

$$Q_0 = 11764.936 \text{ m}^3/\text{s} \quad \text{and} \quad \alpha = 0.23940752 \text{ [-]} \quad (3.14)$$

3.4.3. Sobek discharge frequency curves

The Sobek discharge frequency curves for the Rhine at Lobith for 2085 can be obtained by applying Equation 3.10 and Equation 3.12 to the HBV discharge quantiles (see flowchart in Figure 3.11).

The Sobek discharge frequency curves are presented in Figure 3.14. In the Sobek discharge frequency curves the same patterns can be observed as in the HBV discharge frequency curves (Figure 3.10). However, the median values are lower and the widths of the 95% confidence intervals are smaller for the Sobek discharge frequency curves, in particular for long return periods (see also Tables 3.6 and 3.7). This can simply be explained by the fact that the Sobek-model includes upstream flooding and therefore the discharges entering The Netherlands are much smaller.

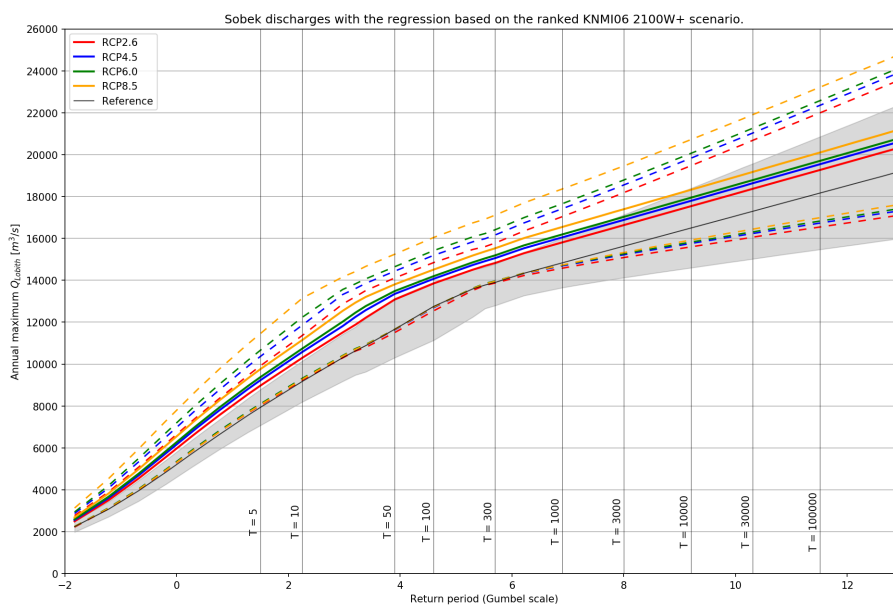


Figure 3.14: Sobek discharge frequency curves for the river Rhine at Lobith in 2085. The regression based on the ordered 2100W+ scenario data (Section 3.4.1) is used to derive the return levels of the Sobek discharges from those of the HBV discharges. The grey area around the reference (black line) represents a 95% confidence region. The dashed lines give the upper and lower bounds of the 95% confidence intervals for HQ_T for each RCP.

Table 3.7: Overview of the discharge extremes presented in Figure 3.14 for a number of return periods in 2085.

Return period [years]	Reference		RCP2.6		RCP4.5		RCP6.0		RCP8.5	
	Median [m ³ /s]	Width Cfd. Int. [m ³ /s]	Median [m ³ /s]	Width Cfd. Int. [m ³ /s]	Median [m ³ /s]	Width Cfd. Int. [m ³ /s]	Median [m ³ /s]	Width Cfd. Int. [m ³ /s]	Median [m ³ /s]	Width Cfd. Int. [m ³ /s]
10	9175	1959	10303	2145	10583	2548	10745	2914	11153	3866
50	11664	2836	13082	2611	13449	2803	13486	2992	13805	3585
100	12757	2776	13854	2306	14073	2502	14198	2681	14513	3331
300	13899	1990	14830	1913	15060	2214	15193	2450	15531	3168
1000	14839	2361	15814	2465	16055	2729	16197	2945	16549	3625
3000	15632	3005	16638	3106	16888	3335	17032	3522	17400	4129
10000	16502	3801	17540	3883	17799	4080	17949	4246	18328	4801
30000	17295	4545	18365	4622	18632	4793	18784	4948	19176	5463
100000	18164	5387	19271	5464	19542	5610	19702	5758	20103	6224

3.4.4. Comparison of the RCP PDFs with the KNMI'14 scenarios

In this section we compare the discharge frequency curves for the RCPs from the previous section, with the ones for the KNMI'14 scenarios. The discharge frequency curves for the KNMI'14 scenarios, presented in Section 3.1.1 (Figure 3.2), are still based on HBV (hydrological) discharges rather than on Sobek (hydrodynamic) discharges. For a fair comparison the KNMI'14 HBV discharges are first converted into KNMI'14 Sobek discharges following the same procedure as for the RCP scenarios, i.e. by applying Eqs. 3.10 and 3.12 to the KNMI'14 HBV discharge quantiles.

Figure 3.15 shows for each RCP scenario the median and the 95% confidence band of the (Sobek) discharge frequency curve together with the (Sobek) discharge frequency curves for the four KNMI'14 scenarios. Note that the four KNMI'14 scenario curves are the same in alle four panels, but that the RCP median and its 95% confidence band differ in each panel.

The range spanned by the four KNMI'14 scenarios for 2085 best corresponds with the 95% confidence range for RCP8.5. For the shortest return periods the range of the KNMI'14 scenarios corresponds to about the 25% to 95% percentage points of the constructed RCP8.5 distribution and for the longest return periods to about the 25% to 85% percentage points (see Table 3.8).

Table 3.8 can also be used to determine the probability that each KNMI'14 scenario is exceeded (or not exceeded) given a certain RCP scenario in 2085. To illustrate this we concentrate on the 1000-year return level. Assuming the RCP2.6 scenario there is a probability of $100 - 49.9 = 50.1\%$ that the 2085GH scenario is exceeded for this return level. Similarly, for the 2085WH scenario this probability is only $100 - 99.9 = 0.1\%$. Assuming the RCP8.5 scenario, the same probabilities become $100 - 21.2 = 78.8\%$ and $100 - 91.7 = 8.3\%$, respectively. Thus even for the most extreme RCP scenario there is still a probability of $\sim 8\%$ that the most extreme KNMI'14 scenario (2085WH) is exceeded. And this probability further increases if larger return levels (or longer return periods) are considered; it becomes e.g. $100 - 81.5 = 18.5\%$ for a return period of 100,000 years, i.e. more than a doubling of the exceedance probability compared to a return period of 1000 years.

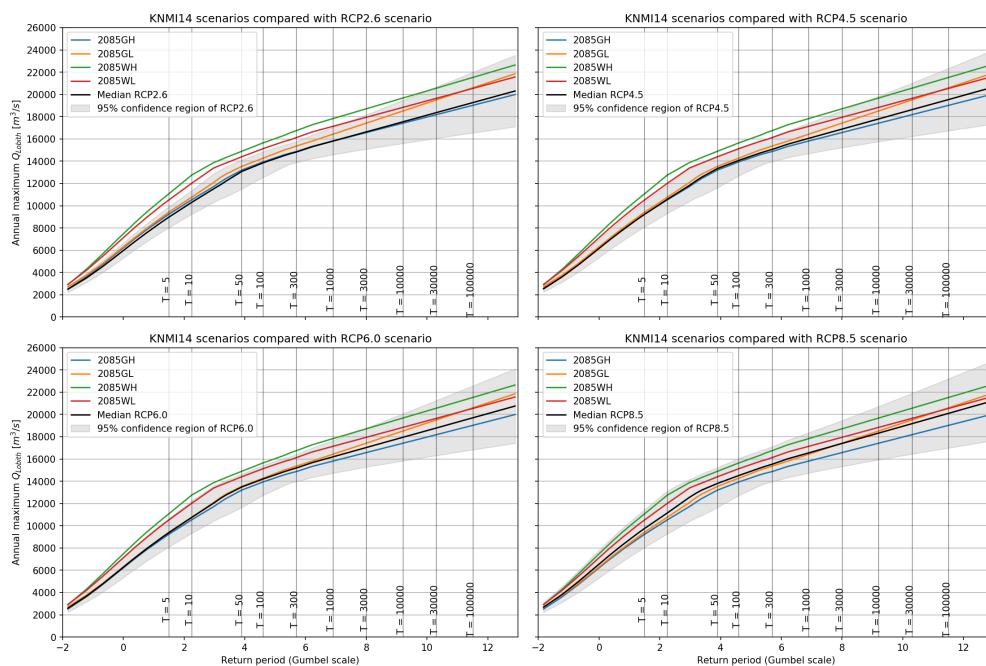


Figure 3.15: Comparison of the (Sobek) discharge frequency curve for each of the four KNMI'14 scenarios with the RCP (Sobek) discharge frequency curve for RCP2.6 (upper left), RCP4.5 (upper right), RCP6.0 (lower left) and RCP8.5 (lower right). The grey area around the RCP curve represents a 95% confidence region.

Table 3.8: Return levels for each KNMI'14 scenario as percentage points of the four RCP scenarios for a number of return periods in 2085. For example, the 10-year return level for the 2085GH scenario corresponds with the 66.2 percentage point of the 10-year return level for the RCP2.6 scenario.

RCP2.6				
Return period [year]	2085GH	2085GL	2085WH	2085WL
10	66.2	80.3	≥ 100.0	99.9
50	62.3	79.2	99.8	98.3
100	57.8	77.9	99.9	98.7
300	53.2	86.4	≥ 100.0	99.6
1000	49.9	83.6	99.9	98.2
3000	47.0	84.0	99.6	95.2
10000	45.0	83.8	98.5	90.5
30000	43.8	83.4	96.9	86.3
100000	43.0	83.1	94.8	82.0

RCP4.5				
Return period [year]	2085GH	2085GL	2085WH	2085WL
10	46.7	61.1	≥ 100.0	98.6
50	47.2	65.3	98.9	94.5
100	43.0	63.8	99.4	95.5
300	36.8	70.5	99.9	97.1
1000	36.2	70.3	99.4	94.0
3000	35.8	73.6	98.4	89.5
10000	35.7	75.4	96.4	84.1
30000	35.7	76.3	94.3	79.7
100000	35.8	77.0	91.7	75.7

RCP6.0				
Return period [year]	2085GH	2085GL	2085WH	2085WL
10	38.5	51.0	99.7	95.6
50	40.2	57.5	97.5	90.7
100	36.4	55.6	98.4	91.7
300	30.2	61.0	99.4	93.3
1000	30.4	62.3	98.6	89.6
3000	30.5	66.8	96.9	84.6
10000	31.2	70.0	94.6	79.5
30000	31.7	71.7	92.0	75.3
100000	32.1	73.1	89.4	71.7

RCP8.5				
Return period [year]	2085GH	2085GL	2085WH	2085WL
10	25.9	34.1	94.6	80.4
50	28.6	41.9	90.0	77.2
100	25.6	39.7	91.2	77.2
300	20.8	42.1	93.4	77.0
1000	21.2	44.7	91.7	73.7
3000	21.8	51.0	89.4	70.0
10000	22.8	56.1	86.6	66.2
30000	23.9	59.6	84.1	63.5
100000	24.8	62.3	81.5	60.8

4

Consequences of the climate uncertainties for the Dike Designs

The Netherlands is protected against river floods by dikes along the rivers. The design of these dikes is highly dependent on the extreme river discharges. The dikes need to withstand the water levels during their entire life span, so the assessment of climate change impact on water levels is important for the design of the dikes. In this chapter, first the flood protection system in The Netherlands is described (Section 4.1), subsequently the uncertainties in the design water levels based on RCP climate scenarios are determined for a few dike sections (Section 4.4) and finally the design water levels based on the RCP scenarios are compared to the design water level based on the KNMI'14 scenarios (Section 4.6).

4.1. Flood protection system in The Netherlands

4.1.1. History

The Netherlands is a low-lying delta area and is therefore sensitive to floods from either the sea or the rivers. The Dutch have a long history in the protection of their land against floods. The first human settlements in the coastal areas were developed in the higher dune areas or on man-made hills, named 'mounds'. Along the rivers, the people lived on the natural levees of the rivers. The rise of the population and increasing importance of agriculture meant that more low-lying areas were utilized. Dikes were constructed to protect these areas. In the 16th and 17th centuries, the Dutch started to reclaim land from the water to create new areas for agriculture and housing. Dikes were built around the water and windmills were used to drain the area. [14]

In the 20th century, a number of large scale events occurred that resulted in large-scale interventions that have changed the Dutch system of water and flood management. In the year 1916, a storm surge flooded areas around the Zuiderzee (currently known as IJsselmeer). After this event a plan was executed to protect this region from flooding by building the Afsluitdijk. This dam turned the Zuiderzee into a lake, the IJsselmeer, by separating the IJsselmeer from the Wadden Sea.

In the year 1953 a storm surge was generated due to a storm on the North Sea in combination with spring tide. It resulted in massive flooding in the south-west part of The Netherlands. The dikes failed at more than a hundred locations, mainly caused by overtopping. The consequences were enormous, 1835 people were killed, thousand of cattle died and billions of guilders of damages occurred. The 1953 disaster also resulted in a change in Dutch flood management. A delta committee was formed, and this committee advised to shorten the coastline by building dams and barriers to close off the estuaries in the south-west of the country. These projects are called the deltaworks and were built between 1953 and 1997. The deltaworks consist of three storm surge barriers, multiple dams and a few locks. The storm surge barrier in the Eastern Scheldt allows part of the tidal flow in normal conditions, but the gates will be closed during storm surges. This barrier is built instead of a dam, so the character and ecology of the estuary won't change too much. The final project of the deltaworks is the Maeslant storm surge barrier near Hook of Holland, which has been finished in 1997. The barrier consists of two movable sector gates that can be floated and closed during storm surges. During normal conditions the gates are open, so the connection between Rotterdam and the North Sea is open for

navigation.

In the years 1993 and 1995 high discharges events occurred in the Meuse and the Rhine river systems. At some places the dikes were just high enough to withstand the water level, but about 250,000 people had to be evacuated. These events resulted in some emergency dike reinforcements and the room for the river program. The principle of this program is that instead of dike reinforcements, measures are preferred to increase the discharge capacity of the river. Examples are the introduction of bypasses, removing obstacles from the river bed and relocating or set back of dikes. The last projects of this program have been finished in 2016. [14]

In the 21st century, no large-scale flood events have occurred so far in The Netherlands. However, some international disasters gave insight in the vulnerability of flood defence systems and the consequences of these disasters. A second delta committee was formed in The Netherlands, to make a plan for the flood protection system for the coming century. The committee gave a number of recommendations, including to update the safety standards. The new safety standards provide a more appropriate protection to the values at risk. These safety standards were introduced in January 2017 and are further discussed in section 4.1.3.

4.1.2. Overview

The Netherlands is a low-lying country, more than 50% of the country is prone to flooding by either the sea or the rivers. These areas are protected by flood defences. In total, the flood defence system in The Netherlands consists of 3600 kilometres of primary flood defences. The primary flood defences prevent flooding from the sea, rivers and large lakes. In addition, the regional flood defences exist along the waterways and canals in polders and smaller lakes. [14]

Before 2017, the flood protection system was divided in so-called dike rings. A dike ring is a system of flood defences and sometimes high grounds that encloses an area in order to protect it against floods. Different types of flood defences can be part of a dike ring. In total there were a 100 dike rings in The Netherlands. For each dike ring a safety standard was expressed by probability of exceedance of a hydraulic load that had to be withstood safely, which can consist of water levels and waves.

Since January 2017 new safety standards have been introduced in The Netherlands. These new safety standards are expressed as the maximum allowable failure probability of flood defences, which enables a more complete assessment of the different failure mechanisms of a flood defence. The new safety standards also take into account the contribution of various dike sections and structures in a dike ring, the safety standard is set for each dike section or structure. Further details about the new safety standards are given in section 4.1.3. [14]

4.1.3. Safety Standards

Safety standards in The Netherlands are expressed by the flood risk. In flood risk management, risk is defined as *a combination of probability and consequence*. The probability of a flood event is generally expressed as the probability per unit time, mostly per year. The consequences can consist of different types of consequences, such as material, ecological damages, injuries and fatalities. The safety standards are formulated as failure probabilities and based on individual, societal and economic risk. [14]

The **individual risk** is the minimum level of safety for citizens living in The Netherlands. The individual risk is the probability a random person loses his/her life at a certain location due to flooding. The potential loss of life given a flood depends on the physical flood characteristic and possibilities to predict and warn for the event, allowing time for evacuation of people. Also the number of people at risk in the flooded area is important for the individual risk. The more people living in the area, the higher the probability in loss of life. The acceptable individual risk in The Netherlands is set to 10^{-5} units.

The **societal risk** refers to the probability of an accident with multiple fatalities. It is often graphically represented by a FN-curve that shows the exceedance probability (F) of the potential number of fatalities (N). The risk is acceptable if the FN-curve for a system does not exceed the limit line. This limit line is derived from the exceedance probability of 1 fatality (base point) and the acceptance of risk (slope). These constants are determined by decision makers.

The **economic risk** is given by an optimal level of safety in terms of an economic optimization. It takes into account the costs of increasing the safety level and reducing the risks. The economic optimization is developed and applied by Van Dantzig [4], to derive the optimal dike height for South Holland after the 1953 disaster. In the economic optimization, the total costs are determined, these costs consist of the investments in a safer system and the net present value of the reduced risk (probability times consequences). The risk can be reduced by constructing a safer system or limiting the damage. The investments become a function of the failure probability of the system, since increasing the safety will lead to an increase of costs. The sum of these two will lead to an optimum, where the total costs are the lowest (see Figure 4.1). [14]

Further information on the derivation of the safety standards is described in the lecture notes of CIE4130 [15] and Vrijling et al. [33].

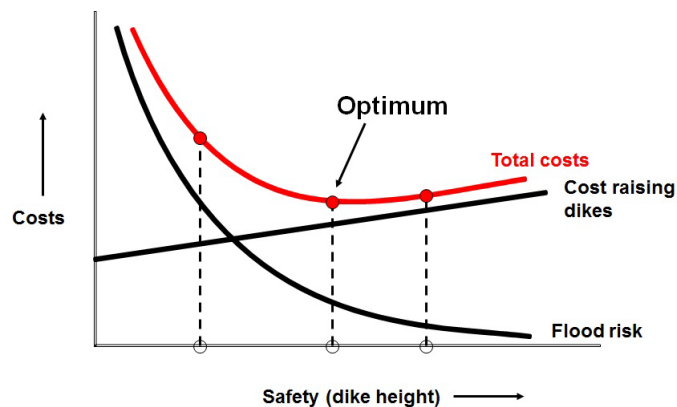


Figure 4.1: Economic Optimization; costs, risk and total costs as a function of the failure probability of the system (source: [15])

Resulting Safety Standards

The three perspectives mentioned above (individual, societal, economic risk) have been applied by the Delta Program to propose the safety standards for primary flood defences in The Netherlands. Based on every perspective, a required failure probability could be determined. The most stringent one determined the safety standard.

The safety standards are given per dike trajectory instead of per dike ring. Studies have shown that the consequences of a dike failure strongly depend on the location of the failure. And a safety standard per dike trajectory can be more location specific than one per dike ring.

The safety standards are divided into norm classes, intervals of the required safety standard are used to determine the corresponding norm class. In The Netherlands two types of norm classes are used, i.e. the '*signaleringswaarde*' and the '*ondergrens (maximale overstromingskans)*'. If the failure probability of the flood defence is below the *signaleringswaarde* action need to be taken to strengthen the flood defence, the *ondergrens* is the maximum acceptable failure probability of the flood defence. The derivation of the required safety standard is made for the *signaleringswaarde*, and the *ondergrens* is in most cases one norm class less strict. Figure 4.2 shows minimum protection levels (the *ondergrens*) of the primary flood defences per trajectory in The Netherlands.

A further description on the derivation of the safety standards in [22].



Figure 4.2: The maximum acceptable failure probability per dike trajectorie (source: [22])

4.2. Basic concepts of Flood Defences

Flood defences are hydraulic structures with the primary objective to provide protection against flooding against the coast, rivers, lakes and other waterways. Different types of flood defences exist, such as a dike, a dam, a storm surge barrier or a dune. Along the river the flood defence system mainly consist of dikes interrupted by hydraulic structures as locks or sluices. In this research only the river section is studied, therefore the focus of the flood defences is on the dikes only. A dike is a water retaining structure consisting of soil with a sufficient elevation and strength to be able to retain the water under extreme circumstances.

4.2.1. Dike profile

Figure 4.3 shows the most importance elements of a typical dike. The dike profile is chosen is such a way to prevent failure of all possible failure mechanisms. The crest level needs to be high enough to withstand extreme water levels. For the expected wave attack a cover layer on the outside of the dike is applied, this revetment can consist of grass, concrete elements, stones or asphalt. The outer berm can be implemented to break and slow down the waves, and the inner berm can be applied to prevent instability and piping. The slopes on the inside and outside have effect on the wave run-up and stability. In section 4.2.2 the failure mechanisms are described in more detail.

The dike core and dike base consist of different type of soils. The composition depends on the location of the dike, which soils exist in the original situation and are available, and it depends on the characteristics of the different soils. Sand and gravel are extremely stable, but also very permeable. Peat is impermeable but is soft, compresses easily and shrinks when it becomes dry. Clay seems the most suitable soil, it is very impermeable but deforms when it gets wet. Many older dikes fully consist of clay. Dikes are nowadays constructed with different types of material, for example a dike core of sand with a clay layer as cover. The benefits of the different soils are used. [14]

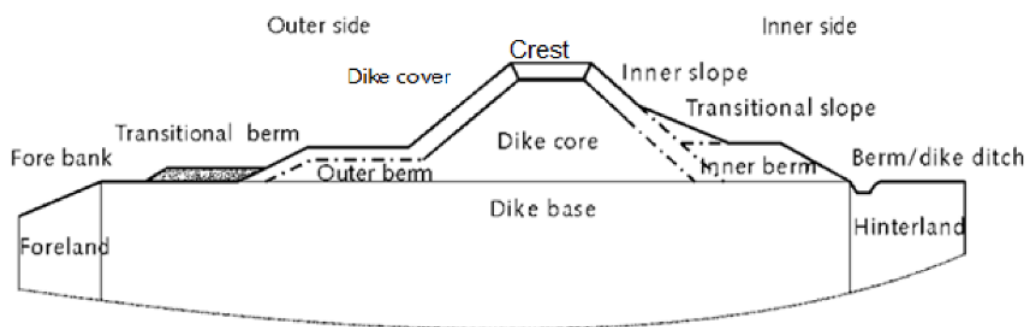


Figure 4.3: General dike profile showing the most important elements (source: [14])

The different dimensions of the dike strongly depend on the design load. Dikes along the coast look different from the dikes along the rivers. Due to the high waves at sea the sea dikes need to have a gentle outer slope, an outer berm and a dike revetment. The waves along the rivers are much smaller, so these elements are not needed. For the river dikes a gentle inner slope is often applied to provide stability during long periods of high water, which is the case during flood waves in the river. On locations where there is not enough land to build the dike some construction, such as sheet piles, can be applied to have a stable dike with a smaller footprint.

4.2.2. Failure mechanisms

For the design of a dike construction the various failure mechanisms needs to be considered. The definition of failure for flood defences is the loss of the water-retaining function. Failure occurs if the load is greater than the resistance.

An overview of the most relevant failure mechanisms is shown in Figure 4.4. Below a description of the five most common failure mechanisms is given.

Overflow of a dike means that the still water level is higher than the crest level of the dike. The overflow itself can lead to flooding of the hinterland or the water flowing down the inner slope can lead to damage and breaching through erosion.

In case of **wave overtopping** the still water level remains below the crest level, but the waves will overflow the dike crest. Failure of the dike is similar as for overflow.

Sliding of the inner slope is a stability problem. As the water level at the outside rises, water infiltrates leading to saturation of the dike body and to increasing pore pressures. The effective stresses reduce and so does the shear strength of the soil, which can lead to the development of sliding planes. To prevent for this failure mechanism a gentle inner slope or an inner berm is applied.

Micro-instability occurs when the seepage water causes the phreatic surface to rise and reach the inner slope of a dike. In case of an impermeable cover layer on the inner slope, the increased pressure inside the dike body can just push off that cover. In case of a permeable inner slope, internal erosion can be initiated.

Piping (or backward internal erosion) occurs if the hydraulic gradients in the subsoil towards the land-side are high. Due the pressure difference water can break through the impermeable cover layer of the hinterland. Soil particles start eroding leading to channels or pipes in the subsoil. These pipes can grow towards the water side of the dike, undermining the foundation of the dike, which can lead to collapse or sliding of the dike body.

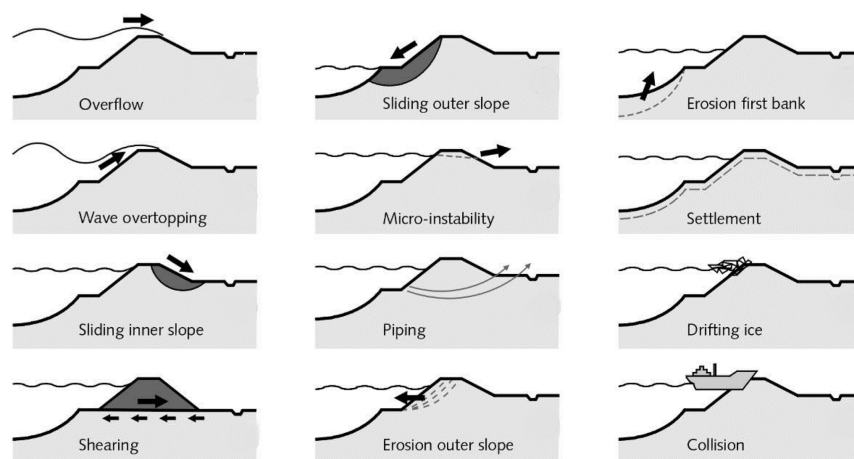


Figure 4.4: Overview of the most relevant failure mechanisms of flood defences (source: [14])

For the design of a dike construction each of the failure mechanisms is considered. The probability of failure for each of the mechanisms is determined. All these probabilities combined give the total probability of failure for the dike section, the total probability needs to be lower than the safety standard.

A detailed description of each failure mechanism is given in the International Levee Handbook [2] and the lecture notes of CIE5314 [14].

4.3. Method to determine the design water level for overtopping

The climate uncertainties in river discharges, as determined in Chapter 3, do have consequences for dike designs. More specifically, these consequences are for the design water levels. For a dike design all the failure mechanisms need to be considered. In this study, however, we only consider the consequences for the design water level for the failure mechanism overtopping. Failure due to overtopping occurs when water flows over the dike crest as a consequence of the water level in the river in combination with wave run up (due to wind). The overtopping results in erosion of the inner slope and finally in breach. In this section the method to determine the design water level for overtopping is described.

In the Netherlands, the allowable probability of failure is determined for a failure mechanism for a cross-section. The starting point is the safety standard of a segment, see Section 4.2. This is translated to an allowable probability of failure for a failure mechanism of a segment through a so-called budget factor. This budget factor is introduced to make sure that all failure mechanisms combined result in a failure probability that is lower than or equal to the standard. This allowable probability of failure for a failure mechanism of a segment is translated to an allowable failure probability of a mechanism of a cross-section using a length-effect factor. This accounts for the length of the segment: the longer the segment, and the higher the contribution of variability in strength, the higher the probability of failure within the segment. Based on this calculated allowable probability of failure, design rules for all failure mechanisms are provided in [26]. Part of the design rules are the so-called 'water level at safety standard', which can be considered a simplification of the design water level for various failure mechanisms.

As mentioned, failure due to overtopping occurs when water flows over the dike due to a combination of the water level and wave run up (due to wind). Climate change does have consequences for the future water levels in the river, but it is assumed that it has no consequences for the wave run up height (due to wind). Therefore, for this study only the water level is of interest and the wave run up is neglected. In the remainder of this study the design water level refers to the water level belonging to overtopping.

The design water level for overtopping can be considered with the mentioned simplification. This simplification, a rule of thumb, tells that the design water level for overtopping is, in good approximation, equal to the water level with an exceedance probability equal to the safety standard [6]. This rule of thumb is valid for cases with a length effect factor of 1, which is a reasonable approximation for overtopping. Hence, in the remainder of this thesis, when the design water level is mentioned, in fact is referred to the design water level based on this rule of thumb. Which is the water level at an exceedance frequency equal to the safety standard.

The design water level can be determined with a relation between the river discharge near Lobith (Q) and the local water level (h), the Q - h relation. This Q - h relation is different for every location along the Rhine. For the design water level the discharge with an exceedance probability equal to the safety standard is selected from the discharge frequency curve (Section 3.4.3) and translated into a water level with the Q - h relation.

The approach to determine the influence of climate effects on the design water level is shown in Figure 4.5. In this approach, the discharge frequency curve and the local safety standard determine the discharge with an exceedance probability equal to the safety standard. Combined with the local Q - h relation, this gives the water level with an exceedance probability equal to the safety standard, which is the definition of the design water level in this thesis.

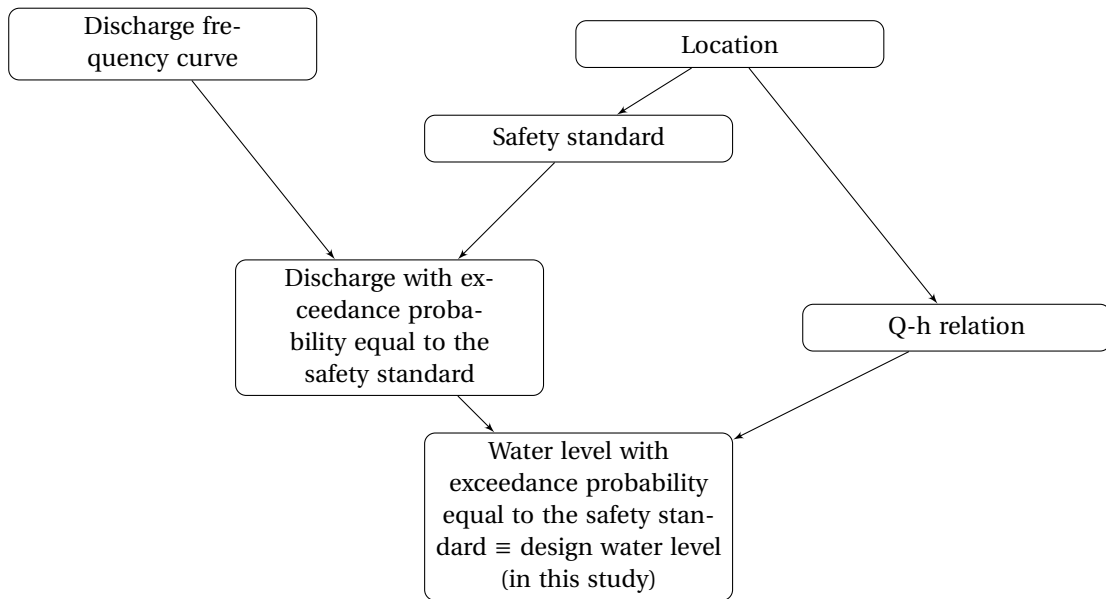


Figure 4.5: Flow chart to determine the design water level for overtopping

Case studies

In this study, the design water level will be determined for four different locations along the river Rhine in The Netherlands. By taking multiple locations the sensitivity of the result to the location and safety standard can be visualized. Therefore, two locations along the Waal branch and two locations along the IJssel branch are chosen. The two locations within the same branch have different safety standards. These locations are chosen in such a way that they lie as close as possible to each other. This ensures that the Q-h relations for these two locations are almost similar, which makes the effect of the difference in the safety standard more clear.

Location 1 and Location 2 are located along the Waal branch (see Figure 4.6). Location 1 is the most downstream part of dike segment 42-1, with a safety standard of 1/10,000 per year. Location 2 is the most upstream part of segment 41-1, with a safety standard of 1/30,000 per year. Location 3 and Location 4 are located along the IJssel branch. These two locations are on the opposite of each other and chosen on one of the smallest points along the IJssel branch. In this case the Q-h relations differ slightly because the locations lie in the inside and outside of a river bend. Location 3 is located within dike segment 49-2, with a safety standard of 1/10,000 per year. Location 4 is located within dike segment 52-1, with a safety standard of 1/3,000 per year.

Table 4.1: Overview of the locations

Location	Dike segment	Branch	Safety Standard [1/year]
1	42-1	Waal	1/10000
2	41-1	Waal	1/30000
3	49-2	IJssel	1/10000
4	52-1	IJssel	1/3000

In Figure 4.7 the Q-h relations of the four locations are given. It can be clearly seen that the relations for the two locations in the Waal branche (Location 1 and Location 2) are almost the same, this is also the case for the two locations in the IJssel branche (Location 3 and Location 4). The differences between the Waal and IJssel branches are, however, significant.

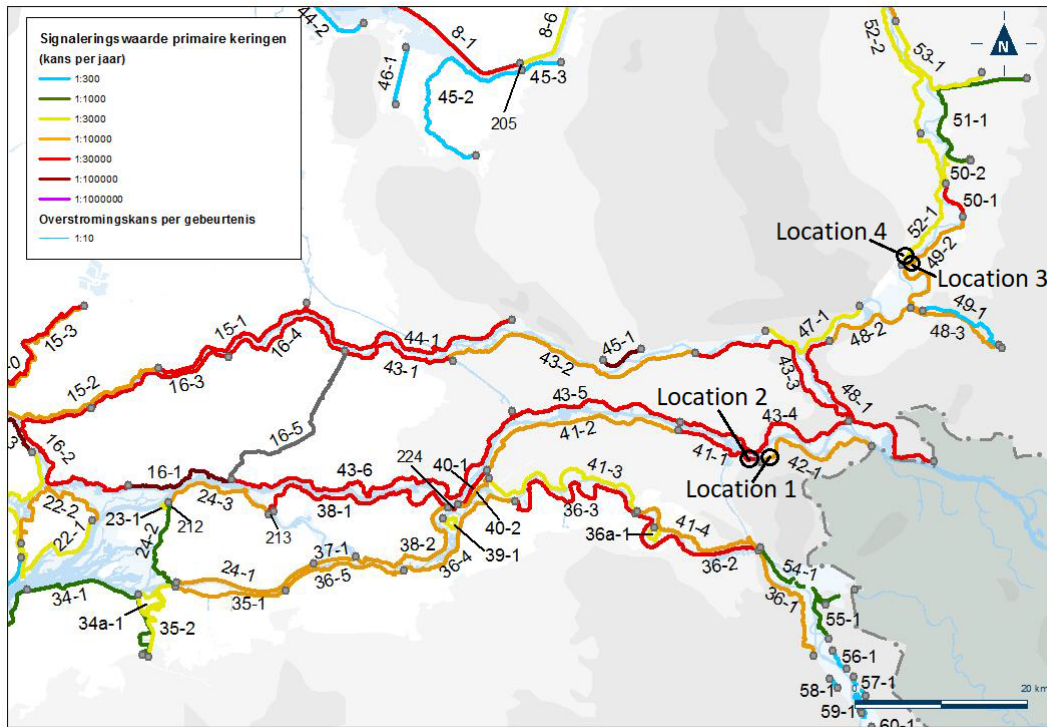


Figure 4.6: The four locations, used in this research, together with the safety standard at these locations.

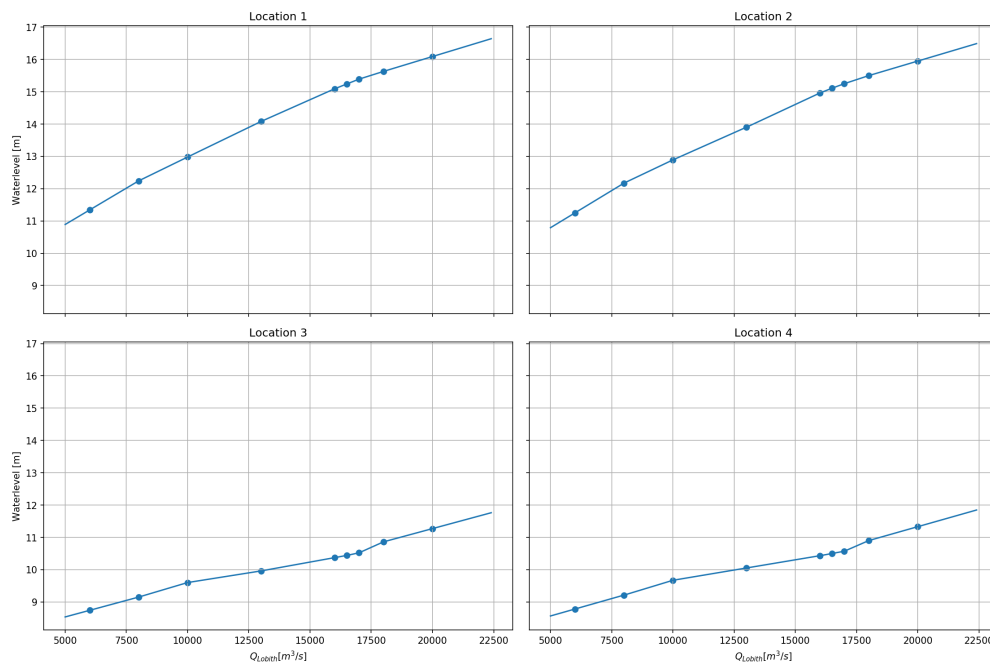


Figure 4.7: Q-h relations for Location 1 (upper left) and Location 2 (upper right) in the Waal branch. And for Location 3 (lower left) and Location 4 (lower right) in the IJssel branch.

4.4. Uncertainty in design water level

This section determines the uncertainty in design water level for different RCP scenarios. The uncertainty in design water level is the consequence of the uncertainty in the discharge return levels as presented in Section 3.4. There are two effects of climate change, modelled as RCP scenarios: the mean of the discharge increases due to the forcing and the uncertainty increases. Both effects will be considered.

The uncertainties in the design water level are determined by sampling a discharge from the discharge distribution with a exceedance probability equal to the safety standard (Figure 3.14), this discharge is subsequently translated into the local water level using the Q-h relation. With a sufficient amount of realizations, a distribution of the local design water level can be constructed. This distribution gives an indication of the uncertainties in the design water level. Since the safety standard and Q-h relation vary per location the results will be different per location as well.

In this section, only the uncertainty in design water level at Location 1 will be discussed, the results for the other three locations is presented in Section 4.5.4. The distributions are constructed per RCP scenario with 10,000,000 realizations of the design water level. Figure 4.8 shows the resulting distributions of the design water level at Location 1 per RCP scenario. The mean values of these distributions are 15.53, 15.60, 15.63 and 15.75 m for RCP2.6, RCP4.5, RCP6.0 and RCP8.5, respectively. This represents the mean effect of the forcing. And the standard deviation is 0.25, 0.26, 0.27 and 0.30 m for RCP2.6, RCP4.5, RCP6.0 and RCP8.5, respectively. Note that the mean of the distributions is the mean of the results of 5 separate samplings with 10,000,000 realizations per sampling.

For the reference situation, which is the situation without climate change, the mean value of the design water level at Location 1 is 15.24 m. So, there is an additional mean height of 0.29 - 0.50 m due to climate change forcing. This range of additional height is the mean forcing scenario uncertainty in the design water level.

The uncertainty in discharge return levels cause an uncertainty in the design water level given a RCP scenario. The latter uncertainty is represented by the standard deviation of the design water level. This standard deviation increases with the forcing of the RCP scenarios. This is something we have noticed for the discharge return levels as well (Chapter 3).

Summarizing the results, there is a mean forcing effect of 0.29 - 0.5 m, depending on the RCP scenario and a variation of 0.2 m due to forcing scenario uncertainty. Within a RCP scenario the width of the 95% confidence interval range of the local water level is 1.00, 1.03, 1.05 and 1.17 m for RCP2.6, RCP4.5, RCP6.0 and RCP8.5, respectively. The variability in the mean of the design water level between the RCP scenarios is thus small compared to the variability for a given RCP scenario.

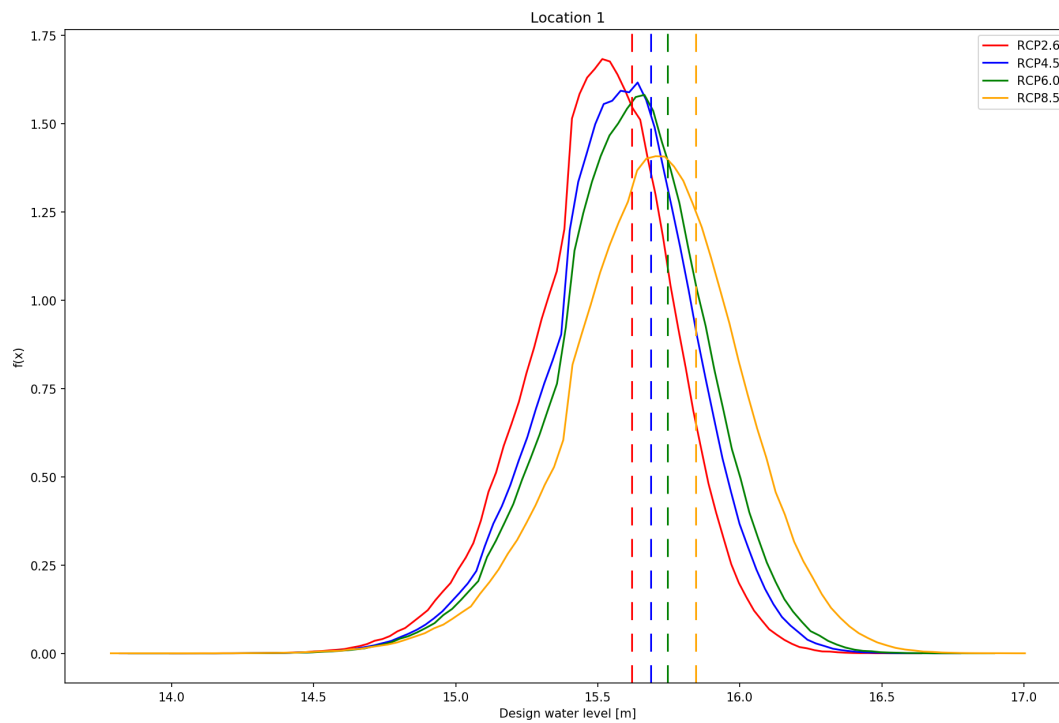


Figure 4.8: PDF of the design water level per RCP at Location 1 (as described in Section 4.4). The dotted vertical lines indicate the design water level with the climate uncertainties integrated (as described in Section 4.5).

4.5. Design water level with integrated uncertainties

The distributions in Figure 4.8 show the uncertainties in the design water level for Location 1 as a result of climate change. But for the design of a dike a single value of the design water level is required. A method to find the single value is to integrate all uncertainties in the discharge frequency curve. This results in a single discharge frequency curve instead of a median discharge frequency curve with an uncertainty band.

4.5.1. Method to integrate the uncertainty

To build these discharge frequency curves the following steps are taken:

1. Sample the probability of exceedance ($1/T$) from a uniform distribution between 0 and 1;
2. Determine the mean and standard deviation of the discharge distribution of the specific RCP with a return period (T) corresponding to the exceedance probability of step 1;
3. Sample a discharge from the normal distribution with the mean and standard deviation of step 2;
4. Repeat steps 1-3 10,000,000 times per RCP. The new discharge frequency curve (with the uncertainties integrated) is constructed from the 10M realizations.
5. Repeat for each RCP

4.5.2. Discharge frequency curves with integrated uncertainties

In Figure 4.9 the resulting discharge frequency curves are presented. These discharge frequency curves can be used to determine the design water level with integrated uncertainties. The discharge with an exceedance probability equal to the safety standard is taken from the discharge frequency curve, and transformed in the design water level by the Q-h relation of the location.

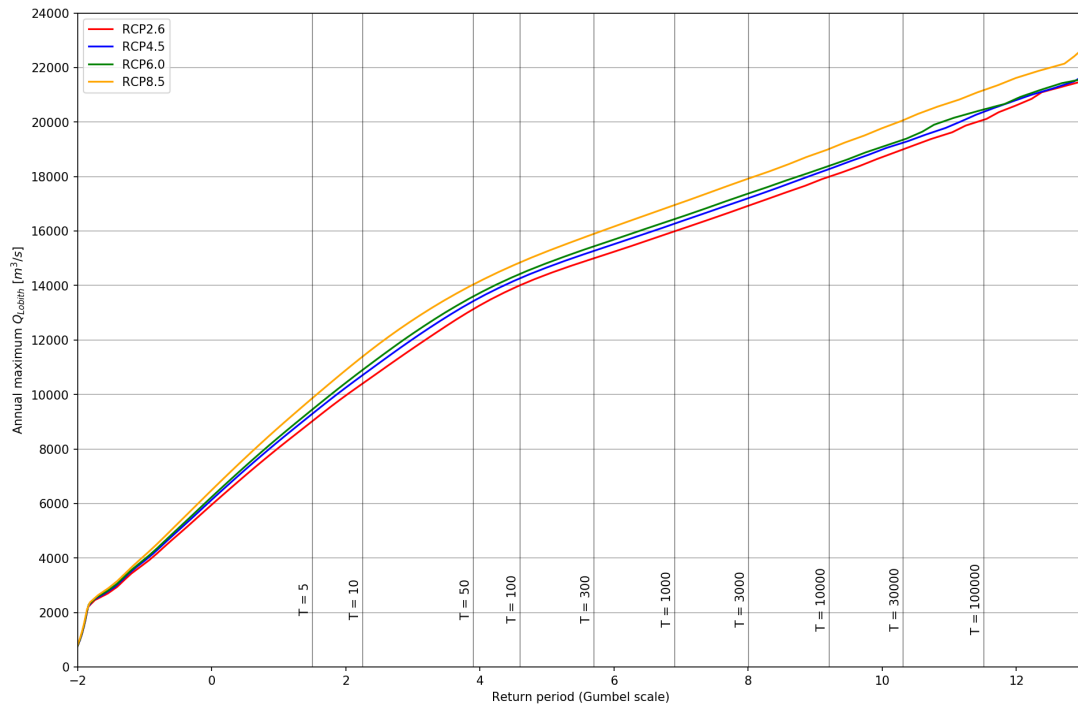


Figure 4.9: Discharge frequency curves of the four RCPs as in Figure 3.14 but with the uncertainties integrated.

4.5.3. Results for Location 1

The safety standard for Location 1 is 1/10,000 per year. For RCP2.6, the discharge with an exceedance probability equal to this safety standard is 17957 m³/s (T=10,000 years in Figure 4.9). Based on Figure 4.7, it can be determined that this corresponds to a local water level of 15.62 m.

The design water level with integrated uncertainties at Location 1 become 15.62, 15.69, 15.75 and 15.85 m for RCP2.6, RCP4.5, RCP6.0 and RCP8.5, respectively. These values are presented in Figure 4.8 with the vertical dotted lines. In this figure it can be seen that these values are slightly higher than the mean of the distribution, which is a logical consequence of integrating the uncertainties. The values of the design water level with the integrated uncertainties corresponds with approximately the 70-percentage point of the design water level distributions for the RCP.

Integrating the uncertainties in the discharge return levels leads to an increase of the design water level of 0.09 to 0.12 m with respect to the mean of the design water level distribution.

4.5.4. Results for the other locations

Also for the other three locations, the distribution of the design water level per RCP and the design water level with integrated uncertainties per RCP are determined. The results for all the locations are shown in Table 4.2. This table gives, for each location, the mean of the distribution and the design water level with integrated uncertainties. These values are given per RCP and for the design water level with integrated uncertainties the design water level as percentage point in its original distribution is given. The reference situation is the case where no climate change is modelled, but where there is still the 'normal' variability present.

The mean value of the distribution of the design water level, which is the mean climate forcing effect, varies per RCP scenario. For Location 1 we have seen that this mean value is an increase of 0.29 - 0.50 m with respect to the mean design water level of the reference situation. For Location 2 and 3 this range is about the same. For Location 4 the increase is in the range of 0.14 to 0.37 m. The increase for Location 4 is lower due to the Q-h relation, which is not a continuous relation (see Figure 4.7). The Q-h relation of Location 3 has the same shape, but the design discharges of the reference and RCPs are in the same continuous part. The difference in mean design level of RCP8.5 and RCP2.6 is about the same for each location, so this is not effected by the location along the Rhine or the safety standard.

Integrating the climate uncertainties of a RCP scenario require an additional water level of 0.09 - 0.12 m to the design water level for Location 1. In Table 4.2 it can be seen that for Location 2 and 3 this range of additional water level is about the same. Only for Location 4 this range is lower, but with a larger spread (0.04 - 0.12 m). This can also be declared by the Q-h relation of Location 4.

The last column in Table 4.2 gives the design water level (with integrated uncertainties) as the percentage point of the original design water level distribution. This percentage point varies between 63% to 73%. The percentage point is higher for the higher RCP scenarios and is slightly different for the four locations. The percentage point gives an indication of the chance that this design water level will be exceeded with that specific RCP scenario. The percentage points indicate that there is a chance of 37% to 27% that the design water level with the integrated uncertainties will be exceeded in 2085, when the same RCP (as used for the design water level) scenario occurs.

Table 4.2: Overview of the design water level of each location and for all RCP scenarios.

Location	Scenario	Mean design water level [m]	Design water level with integrated uncertainties [m]	Design water level as percentage point in its original distribution
1	Reference	15.24		
	RCP2.6	15.53	15.62	67
	RCP4.5	15.60	15.69	68
	RCP6.0	15.63	15.75	67
	RCP8.5	15.75	15.85	72
2	Reference	15.32		
	RCP2.6	15.61	15.72	70
	RCP4.5	15.68	15.78	70
	RCP6.0	15.72	15.84	70
	RCP8.5	15.82	15.95	73
3	Reference	10.44		
	RCP2.6	10.72	10.85	67
	RCP4.5	10.82	10.91	68
	RCP6.0	10.87	10.95	67
	RCP8.5	10.97	11.06	71
4	Reference	10.38		
	RCP2.6	10.52	10.56	63
	RCP4.5	10.56	10.63	65
	RCP6.0	10.59	10.70	65
	RCP8.5	10.75	10.87	69

4.6. Comparison of design water level with the KNMI'14 climate scenarios

The design water level based on the KNMI'14 scenarios can be obtained with the same method as is used for the RCPs. In Section 3.4.4 the discharge frequency curves of all KNMI'14 climate scenario in 2085 are presented. The individual KNMI'14 discharge frequency curves do by definition not include climate model uncertainty, but there is still uncertainty involved. It is assumed that this uncertainty is equal to the uncertainty for the reference situation (i.e. uncertainty in natural variability, hydrological model and hydraulic model).

Since Table 4.5.4 shows that for three of the four locations the increase in the mean design water level with respect to the reference situation is almost similar. The design water level for KNMI'14 is therefore only considered for Location 1.

For the KNMI'14 scenarios we start with the discharge frequency curves of these KNMI scenarios and the uncertainties in these curves due to natural variability and hydrological/hydraulic uncertainty. The uncertainties in the discharge return levels are integrated with the same method as for the RCP scenarios described in Section 4.5.1. This results in four new discharge frequency curves, one for each KNMI'14 scenario. From these the discharges with a exceedance probability equal to safety standard (for Location 1 the 10,000-year return level) are taken. With the Q-h relation for Location 1 the design water level is determined. The resulting design water levels for the KNMI'14 scenarios at Location 1 are presented in Figure 4.10 and Table 4.3.

The design water level of 15.60 m for the lowest KNMI'14 scenario (2085GH) is almost equal to the 15.62 m for the lowest RCP scenario (RCP2.6). And the design water level of 16.11 m for the highest KNMI'14 scenario (2085WH) is 0.26 m higher than the 15.85 m for the highest RCP scenario (RCP8.5). The design water level for the RCP8.5 scenario corresponds most closely to the 15.82 m for the KNMI'14 2085GL scenario.

Table 4.3 also presents for the KNMI'14 scenarios the design water level as percentage points of the design water level distributions for the RCPs. The associated probability gives the chance that the design water level will not be exceeded in 2085, given that RCP scenario. It can therefore be used to say something about the chance that the dike does not meet the safety requirements of overtopping in 2085. There is chance of 38% that dike with the KNMI'14 GH scenario will not meet the safety standards in 2085 if RCP2.6 occurs, when RCP8.5 occurs this chance is 65%. The WH scenario requires the highest design water level, this will therefore be a safe solution. The chance that this design water level does not meet the safety standard in 2085 is less than 10% for all the RCPs.

Table 4.3: Comparison between the KNMI'14 climate scenarios and RCP scenarios for the design water level at Location 1

	Design water level based on KNMI'14 scenarios [m]	Design water level based on the KNMI'14 scenarios as percentage points of the design water level distribution for			
		RCP2.6	RCP4.5	RCP6.0	RCP8.5
GH	15.60	62	52	46	35
GL	15.82	91	85	80	67
WH	16.11	99	99	98	92
WL	15.91	90	91	88	76

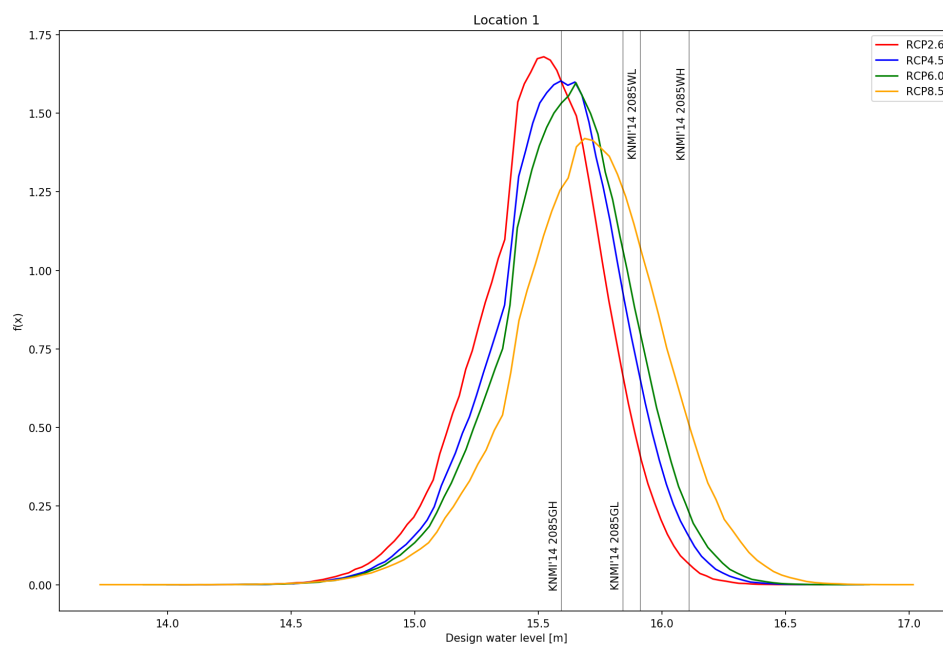


Figure 4.10: As Figure 4.8 but with the design water level for the four KNMI'14 climate scenarios (vertical lines) compared with the distribution of the design water level of the RCPs at Location 1

5

Discussion

In this Chapter some of the methods used in this study and the consequences of these methods on the results are discussed. Only the most relevant assumptions made in the methods are discussed. The first relevant assumption is the use of the regression lines to determine the climate uncertainties in the future extreme river discharges. These regression lines are easy to use and reduce the amount of work significantly, but the use of the regression lines may have consequences for the results. The regression lines are further discussed in Section 5.1.

The second assumption is made in the method to determine the consequences of the uncertainties in discharge return levels on the design water level. It is assumed that the design water level for the failure mechanism overtopping gives an indication on the consequences for the required dike dimensions. In Section 5.2 it is discussed if this is a reasonable assumption.

5.1. Regression lines

Two different regression lines are used in this research (see flowchart in Figure 3.1). The first regression line is used to determine the change in the extreme discharge for a given return period (dHQ_T) from the change in the mean annual maximum discharge ($dMHQ$) of a data series. The other regression line is to transform the quantile of the hydrological annual maximum discharge ($HQ_{T,HBV}$) into a quantile of the hydrodynamic annual maximum discharge ($HQ_{T,Sobek}$). Both regression lines are discussed in the remainder of this section.

dMHQ-dHQ regression line

As already mentioned above the first regression line in this research is used to determine the dHQ_T for any return period. A relation between $dMHQ$ and dHQ_T , as given in Section 3.1.2, is used for this regression. Below here we first discuss the decisions made for this relation and thereafter we discuss the uncertainties in this relation.

The data used for the regression line come from the long discharge simulations for the eight KNMI'14 scenarios. These eight KNMI'14 climate scenarios (four for 2050 and four for 2085) provide the discharge responses to eight different climate forcings. All eight simulations have a length of 50,000 years and the resulting annual maximum discharges calculated with both the hydrological model HBV and hydrodynamic model Sobek are sufficient to reliably determine both $dMHQ$ and dHQ_T (for T up to 100,000 years).

The regression relation is based on the HBV annual maxima since it is used to estimate the dHQ_T 's from a large ensemble of HBV simulations using the climate projections from various climate models and four different RCP scenarios (see Section 3.2 for details). These short HBV simulations (of only 56 years) are denoted as the short series. From these short series $dMHQ$ can be calculated, but they are too short to reliably determine the required dHQ_T .

The relation between $dMHQ$ and dHQ_T is taken to be linear through the origin. It seems reasonable to assume that if there is no change in the MHQ (no response in the mean of the annual maxima) there is also

no change (response) in the HQ_T 's. It is therefore a logical assumption that the regression goes through the origin. Figure 3.3 confirms this, in particular for the shorter return periods.

The slope of the linear relation is however uncertain, which results in an uncertainty in the dHQ_T as well. To account for this uncertainty the standard error of the slope is given in Table 3.1 for four return periods. The table shows that this standard error increases with the return level. The standard error is relatively small (even for the long return levels) and therefore the uncertainty in dHQ_T due to the uncertainty in the slope of this regression line is also small. This uncertainty is still included in the total uncertainty in HQ_T (see flowchart in Figure 3.8), but compared with other uncertainties in HQ_T the additional uncertainty due to this regression line is almost negligible.

Regression HBV-Sobek

Another regression line is used to obtain the Sobek (hydrodynamic) discharge from the HBV (hydrological) discharge (see Section 3.4.1). The use of this regression line saves a lot of computationally expensive calculations with the Sobek model. This is also the reason that a HBV-Sobek regression is used in the Dutch design guideline (Ontwerpinstrumentarium 2014 (OI2014)) as well.

As mentioned in Section 3.4.1, in this research we do not use the same regression line as used in OI2014. The regression used in OI2014 is based on the original pairs of HBV and Sobek annual maximum discharges. Such a regression can be used to obtain individual Sobek discharges from individual HBV discharges. However, in this study, only the quantiles of the annual maximum HBV discharges are available (the HQ_T) and not the individual annual maxima. For a suitable relation to convert these quantiles it is necessary to regress the quantiles of the Sobek discharges on the quantiles of the HBV discharges, as shown in Figure 3.12. For this regression the data sets of both the Sobek and HBV discharges are ordered in an increasing sequence, so that the highest Sobek discharge is plotted against the highest HBV discharge (the lowest Sobek against the lowest HBV, etc.).

Another point of discussion is about the data set that can be best used for this regression. The regression used in OI2014 is based on the data set of the KNMI'06 2100W+ climate scenario. This is however not the most recent climate scenario and the data sets with both HBV and Sobek discharges are also available for the KNMI'14 climate scenarios. The discharges of the KNMI'14 climate scenarios are also simulated with more recent versions of the HBV and Sobek models. It's therefore preferable to use one of the KNMI'14 climate scenarios for the regression. There are however a few concerns about these data sets, and therefore it is better to use the KNMI'06 scenario instead of one of the KNMI'14 scenarios.

In Figure 5.1 the relation between the quantiles of the Sobek discharges and quantiles of the HBV discharges is given for the KNMI'14 2085WH scenario. What immediately stands out at this regression line is the difference in shape compared with the regression line in Figure 3.12. The regression line in Figure 3.12 becomes less steep for large discharges, which is due to upstream flooding. Also the regression line in Figure 5.1 becomes less steep at about the same point ($Q_{HBV} \sim 14000 \text{ m}^3/\text{s}$), but starts to become steep again for the extreme discharges ($Q_{HBV} \geq 19000 \text{ m}^3/\text{s}$). A possible explanation for this behaviour is that at a certain point the flood plains have no more capacity and then the river discharge may further increase. A group of experts concluded, however, that it is impossible to have such high discharges in the Rhine at Lobith [5]. It is therefore questionable if the behaviour in the regression line in Figure 5.1 is realistic or that there are some errors in the used models. Since it is not fully clear what causes this shape of the regression line and since the experts have more confidence in the behaviour shown in the curve based on the KNMI'06 2100W+ scenario (Figure 3.12), the regression line based on this scenario is used in this study.

The last thing we want to discuss is the reliability of the regression line. Figure 3.12 shows that there is almost no scatter around the regression line. This is a result of the ordering of the data. It does not mean, however, that the uncertainty of the regression line is small. One way to estimate this uncertainty is to resample from the original pairs of HBV and Sobek annual maximum discharges and to refit the regression relation on the ordered resampled data. Note that resampling should not be based on the ordered data in Figure 3.12 because of their dependence.

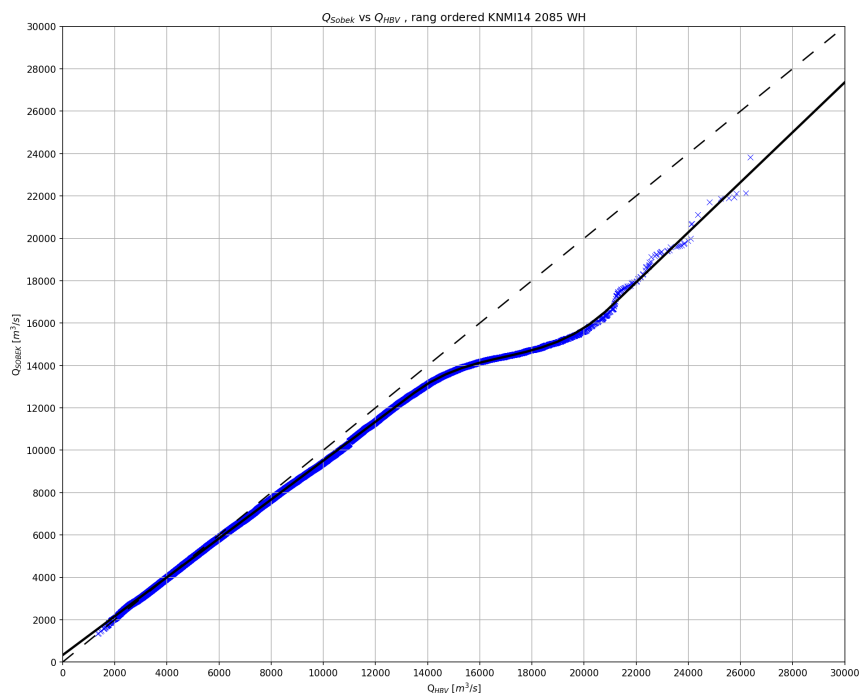


Figure 5.1: Relation between the discharges from the hydrological model HBV and the hydraulic model Sobek. Based on the ordered data of the KNMI'14 2085 WH scenario.

5.2. The consequences of the climate uncertainties on design water levels

In this study only the consequences of the climate uncertainties on the design water levels for the failure mechanism overtopping are considered. Whether these design water levels are representative for the consequences of the climate uncertainties on the total dike dimensions is discussed in this section.

First, the consequences of neglecting the wave run-up in the design load for overtopping is discussed. This design load is a combination of the water level and wave run-up (due to wind). It is, however, assumed that the wave run-up does not change for the future climate. The change in design load for the future climate is only caused by the change in the water level return levels. Therefore, the results for the change in design water level and the consequences of the climate uncertainties on this design water level are the same for the results and consequences for the design load. This means that there are no consequences for the results of the design load if the wave run-up is neglected.

The water level is an important load parameter for most of the failure mechanisms. The return level of the design water level differ slightly per failure mechanisms, due to the different budget factors. This study has shown that the consequences for the design water level do not vary much per location, and thus do not vary much for different safety standards or the return level of the design water level. The consequences of climate change on the increase in design water level and the uncertainties in this design water level will therefore be the same for the design water level of other failure mechanisms as it is for overtopping. However, it can not be said that the consequences of the climate change for the other failure mechanisms are the same as for overtopping. For overtopping the water level is the only load parameter effected by climate change. This is not the case for all failure mechanisms. For example, the duration of the flood wave is of great interest for piping. This duration will be different for the future climate, but is not considered in this study. Therefore, the results of this study do not give a good indication of the consequences of climate change for piping.

The next thing to discuss is the effect of the design water level for overtopping on the dike dimensions. To prevent failure due to overtopping there are two solutions possible; the dike can be heightened or measures to reduce the wave run-up can be taken. An increase in the design water level (and thus in design load) is therefore not always the same as the extra required dike height. In some cases it is possible to take in the additional

design load by applying extra measures to reduce the wave run-up. In most cases, however, the dike height need to increase due to the increase in design water level. The consequences of climate change on the design water level therefore give a good indication for the consequences on the required dike height for overtopping.

The failure mechanism overtopping is for most of the Dutch dikes the most important. When the dike is high enough to prevent failure due to overtopping, it is in these cases also high enough to prevent failure due to overflow. The results for the design water level for overtopping therefore give a good indication for the consequences of the total required dike height. However, the dike height is not the only element of a dike cross section. Some elements do have a strong correlation with the dike height. For example, when the dike height increases the width of the dike must increase as well to prevent stability problems. The dike height gives an indication of the total dike dimensions, yet there are still elements which are not effected by the dike height.

It can be concluded that the consequences of climate change on the design water level for overtopping gives a good indication for the consequences on the design water level. The consequences for some other failure mechanisms can be different however, since not all designs loads effected by climate change are considered in this study. The consequences for the design water level for overtopping also gives an indication for the required dike height, but not for the dimensions of all dike elements. It is necessary to consider all the failure mechanisms to determine the consequences for the other dike elements.

6

Conclusions and Recommendations

6.1. Conclusions

This section presents the conclusions of the report. With these conclusions the research questions as given in Section 1.3 are answered.

There are multiple sources of uncertainty in extreme river discharges. Not all these sources are the consequence of climate change, some of them already exist for the river discharges of the current climate. Climate change, however, makes the uncertainties in the river discharge larger for the future climate than for the current climate.

The uncertainty in the river discharges of the reference situation (the current climate) is caused by natural variability and hydrological uncertainty. Table 3.7 shows that these uncertainties in river discharges (represented by a 95% confidence range) vary per return period. For the 1000-year return level the confidence range is 2361 m³/s, while the confidence range for the 10,000-year return level is 3801 m³/s.

In the future river discharges there are two additional sources of uncertainty, namely the forcing scenario uncertainty and uncertainty in the response to this forcing (i.e. climate model uncertainty). The discharge frequency curves of the river discharge in 2085 for the four different forcing (RCP) scenarios show that both the mean response in the return levels and its uncertainty (the width of the confidence intervals) increase with the RCP forcing. And this is consistent with the LME-model (for dMHQ) which has a fixed forcing effect and a random climate model effect that both depend on the forcing. For the 10,000-year return level the increase with respect to the reference situation in the median value ranges from 1038 m³ for RCP2.6 to 1826 m³/s for RCP8.5. These increases do not depend much on the return period; the difference in response between the RCP8.5 and RCP2.6 scenario is 788 m³/s for the 10,000-year return level and 735 m³/s for the 1000-year return level (Figure 3.14 and Table 3.7).

In addition to the forcing scenario uncertainty the width of the 95% confidence interval for a particular return level (and thus the uncertainty in the response) increases due to climate change as well. As already said, also the uncertainty in the response depends on the RCP forcing (and this follows from the LME-model). For the 10,000-year return level the width of the 95% confidence interval increases from 3883 m³/s for RCP2.6 to 4801 m³/s for RCP8.5. Compared with the 3801 m³/s for the reference situation (the current climate) this means an increase in the width of the 95% confidence interval of 82 and 1000 m³/s for RCP2.6 and RCP8.5 respectively. The difference between this increase of 918 m³/s for the two RCPs is of the same order, and actually somewhat larger than the difference of 788 m³/s in their mean response. For other return levels a similar result is obtained.

Figure 3.15 shows that the four KNMI'14 scenarios for 2085 fit best in the 95% confidence region of the RCP8.5 scenario. However, for long return periods (i.e. > 10,000 years) the 95% confidence region of RCP8.5 becomes much wider than the range described by the KNMI'14 scenarios. For the other three RCP scenarios the KNMI'14 scenarios are mainly located in the upper half of the 95% confidence interval. This indicates that

there is a large chance (i.e. > 50%) that the KNMI'14 scenarios will never be exceeded in 2085 under these RCP scenarios.

The uncertainties in the discharge return levels do have consequences for the water levels used for the flood protection designs, denoted as the design water levels. For Location 1 the distributions of the design water level for the failure mechanism overtopping have a standard deviation of 0.25, 0.26, 0.27 and 0.30 m for RCP2.6, RCP4.5, RCP6.0 and RCP8.5, respectively. And the mean values for these distributions are 15.53, 15.60, 15.63 and 15.75 m for RCP2.6, RCP4.5, RCP6.0 and RCP8.5, respectively. The mean design water level for the reference situation at this location is 15.24 m, so there is an increase of 0.29 - 0.50 m in the mean design water level due to the response of the RCP scenario forcing. The mean response to the forcing and the uncertainty in the response expressed by the standard deviation are of the same order of magnitude. For Location 2 and Location 3 a similar range in the mean response of the design water level is found, and for Location 4 the response is somewhat lower. Thus the different locations along the Rhine and safety standard does not have much effect on the response in the increase in design water level.

For each RCP the uncertainties in the discharge return levels are integrated into a single value for the design water level. This resulting design water level is 0.08 - 0.13 m higher than the mean design water level for the RCPs. This increase in design water level is of the same order for Location 1, Location 2 and Location 3. For Locations 4 the range of this increase is somewhat large, namely 0.04 - 0.12 m.

The design water level for the KNMI'14 scenarios is only considered for Location 1. For the KNMI'14 scenarios the design water level is only determined with integrated uncertainties. Compared to the design water levels with integrated uncertainties for the RCP scenarios, the design water level for the most extreme KNMI'14 scenario (2085WH) is 0.26 m higher than the design water level for the most extreme RCP scenario (RCP8.5). The design water level for the lowest KNMI'14 scenario (2085GH) is almost the same as the one for the lowest RCP scenario (RCP2.6).

Comparing the design water level for the KNMI'14 2085WH scenario with those for the RCP scenarios, shows that there is an exceedance probability of only 1% to 8% (depending on the RCP scenario) for this water level in 2085. For the other KNMI'14 scenarios this exceedance probability clearly increases, with a maximum of 65% for the KNMI'14 2085GH scenario assuming RCP8.5 (see Table 4.3).

6.2. Recommendations

In this section we would like to recommend some points for following studies.

Determine the uncertainty of the HBV-Sobek regression.

In this study this uncertainty is not determined, but it is a methodological uncertainty that contributes to the overall uncertainty of the future extreme river discharges. This becomes relevant in particular when the long simulations with the new version of Sobek, that better includes flooding in the lower Rhine area, become available. These are also the Sobek simulations that are planned to be used for the next update of OI (OI2018).

Determine the dike dimensions when taking all the failure mechanisms into account.

In this study only the consequences of the uncertainties in the future extreme river discharges on the local water levels were determined. The local water level is of great importance for most of the failure mechanisms and is therefore a good first indication of the consequences of the climate uncertainty for the required dike dimensions. But to determine the real consequences for the required dike dimensions all the failure mechanisms need to be considered. This is also what is required by the Dutch design guideline.

Determine the development of the uncertainties in time.

In this study we have only considered the uncertainties in the river discharge in 2085. The forcing of the RCPs however changes over time (see Figure 2.4), and since the uncertainties depend on the amount of forcing these uncertainties will develop over time. For dike design consideration this change over time is interesting. For example, when the change of the uncertainties over time is known, the chance can be computed that the dike does not meet the safety standard any more. This can be done for each future year, while in this research it is only done for 2085. When these chances are known they can be used to determine the dike dimensions. For situations where it is not desirable to reinforce the dike before the end of its lifetime, the dike needs to be designed in such a way that this chance is small during its entire lifetime.

Bibliography

- [1] T. Adri Buishand and Theo Brandsma. Multisite simulation of daily precipitation and temperature in the Rhine Basin by nearest-neighbor resampling. *Water Resources Research*, 37(11):2761–2776, 2001. ISSN 1944-7973. doi: 10.1029/2001WR000291. URL <http://dx.doi.org/10.1029/2001WR000291>.
- [2] CETMEF, CIRIA, and USACE. *The International Levee Handbook*. CIRIA C 731, 2013.
- [3] U. Cubasch, D. Wuebbles, D. Chen, M.C. Facchini, D. Frame, N. Mahowald, and J.G. Winther. *Chapter 1: Introduction*. In: *Climate Change 2013: The Physical Science Basis. Contribution of Working Group I to the Fifth Assessment Report of the Intergovernmental Panel on Climate Change [Stocker, T.F., D. Qin, G.-K. Plattner, M. Tignor, S.K. Allen, J. Boschung, A. Nauels, Y. Xia, V. Bex and P.M. Midgley (eds.)]*. Cambridge University Press, 2013.
- [4] D. Van Dantzig. Economic decision problems for flood prevention. *Econometrica*, 24(3):276–287, 1956. ISSN 00129682, 14680262. URL <http://www.jstor.org/stable/1911632>.
- [5] Huib J. de Vriend, Matthijs Kok, Joost Pol, and Mark Hegnauer. *Heeft de Rijnafvoer bij Lobith een maximum?* Expertisenetwerk Waterveiligheid, 2016.
- [6] Matthijs Duits and Bob Maaskant. *Resultaten illustratiepunten*. HKV Consultants, 2015. PR3134-memorandum.
- [7] Martin Hanel and T. Adri Buishand. Assessment of the Sources of Variation in Changes of Precipitation Characteristics over the Rhine Basin Using a Linear Mixed-Effects Model. *Journal of Climate*, 28:6903–6919, 2015.
- [8] M. Hegnauer. *Afvoerstatistiek Ontwerp Instrumentarium (OI) 2014*. Deltares Report 1220042-004-ZWS-0001, 2015.
- [9] M. Hegnauer, J.J. Beersma, H.E.P. Van den Boogaard, T.A. Buishand, and R.H. Passchier. *Generator of Rainfall and Discharge Extremes (GRADE) for the Rhine and Meuse basins: final report of GRADE 2.0*. Deltares Report 1209424-004-ZWS-0018, Delft, The Netherlands, 2014.
- [10] Mark Hegnauer and Anke Becker. *Technical Documentation GRADE part II: Models Rhine*. Deltares Report 1207771-003-ZWS-0013, Delft, The Netherlands, 2013.
- [11] IPCC. *Climate Change 2007: The Physical Science Basis. Contribution of Working Group I to the Fourth Assessment Report of the Intergovernmental Panel on Climate Change [Solomon, S., D. Qin, M. Manning, Z. Chen, M. Marquis, K.B. Averyt, M. Tignor and H.L. Miller (eds.)]*. Cambridge University Press, 2007.
- [12] IPCC. *Climate Change 2013: The Physical Science Basis. Contribution of Working Group I to the Fifth Assessment Report of the Intergovernmental Panel on Climate Change [Stocker, T.F., D. Qin, G.-K. Plattner, M. Tignor, S.K. Allen, J. Boschung, A. Nauels, Y. Xia, V. Bex and P.M. Midgley (eds.)]*. Cambridge University Press, 2013. doi: 10.1017/CBO9781107415324.
- [13] IPCC. *Summary for Policymakers In: Climate Change 2013: The Physical Science Basis. Contribution of Working Group I to the Fifth Assessment Report of the Intergovernmental Panel on Climate Change [Stocker, T.F., D. Qin, G.-K. Plattner, M. Tignor, S.K. Allen, J. Boschung, A. Nauels, Y. Xia, V. Bex and P.M. Midgley (eds.)]*. Cambridge University Press, 2013.
- [14] S. N. Jonkman, R. E. Jorissen, T. Schweckendieck, and J. P. Van den Bos. *Flood Defences - Lecture Notes CIE5314*. Delft University of Technology, 2017.
- [15] S.N. Jonkman, R.D.J.M. Steenbergen, O. Morales-Nápoles, A.C.W.M. Vrouwenvelder, and J.K. Vrijling. *Probabilistic Design: Risk and Reliability Analysis in Civil Engineering - Lecture Notes CIE4130*. Delft University of Technology, 2015.

- [16] KNMI. *KNMI Climate Change Scenarios 2006 for the Netherlands* [B. van den Hurk, A. Klein Tank, G. Lenderink and others]. KNMI, De Bilt, The Netherlands, 2006. Scientific Report WR2006-01.
- [17] KNMI. *KNMI'14: Climate Change Scenarios for the 21st Century - a Netherlands Perspective* [B. van den Hurk, P. Siegmund, A. Klein Tank (Eds) and others]. KNMI, De Bilt, The Netherlands, 2014. Scientific Report WR2014-01.
- [18] P. Kraaijenbrink. *Advanced Delta Change method: Extension of an application to CMIP5 GCMs*. KNMI, 2013. Internal report; IR 2013-04.
- [19] G. Lenderink and J. Beersma. *The KNMI'14 $W_{H,dry}$ scenario for the Rhine and Meuse basins*. KNMI, De Bilt, The Netherlands, 2015. KNMI Scientific Report WR 2015-02.
- [20] G. Lenderink, B.J.J.M. van den Hurk, A.M. G. Klein Tank, G.J. van Oldenborgh, E. van Meijgaard, H. de Vries, and J.J. Beersma. Preparing local climate change scenarios for the Netherlands using re-sampling of climate model output. *Environmental Research Letters*, 9:115008 (13pp), 2014.
- [21] Malte Meinshausen, S. J. Smith, K. Calvin, J. S. Daniel, M. L. T. Kainuma, J-F. Lamarque, K. Matsumoto, S. A. Montzka, S. C. B. Raper, K. Riahi, A. Thomson, G. J. M. Velders, and D. P. P. van Vuuren. The RCP greenhouse gas concentrations and their extensions from 1765 to 2300. *Climatic Change*, 109:213–241, 2011.
- [22] Ministerie van Infrastructuur en Milieu. *Achtergronden bij de normering van de primaire waterkering in Nederland - Hoofdrapport*. 2016.
- [23] A Paarlberg. *GRADE Niederrhein: Dijkoverstroming versus dijkdoorbraak*. HKV report PR2942.10, Lelystad, 2014.
- [24] José C. Pinheiro and Douglas M. Bates. *Linear Mixed-Effects Models: Basic Concepts and Examples*. Springer, 2000. ISBN 0-387-98957-9.
- [25] Geert Prinsen, Henk van den Boogaard, and Mark Hegnauer. *Onzekerheidsanalyse hydraulica in GRADE*. Deltares Report 1220082-010-HYE-0001, Delft, The Netherlands, 2015.
- [26] Rijkswaterstaat Water, Verkeer en Leefomgeving. *Handreiking Ontwerpen met Overstromingskansen - Veiligheidsfactoren en Belastingen bij nieuwe Overstromingskansnormen (OI2014)*. 2017.
- [27] K.M.F. Rijnen. *The Influence of Sea Level Rise Uncertainties on Flood Design Considerations*. Delft University of Technology, 2016. Master Thesis.
- [28] M.J. Schmeits, E.L.A. Wolters, J.J. Beersma, and T.A. Buishand. *Rainfall generator for the Rhine basin: Description of simulations using gridded precipitation datasets and uncertainty analysis*. Koninklijk Nederlands Meteorologisch Instituut, 2014. KNMI publication 186-VII.
- [29] F.C. Sperna Weiland, M. Hegnauer, L.J.E. Bouaziz, and J.J. Beersma. *Implications of the KNMI'14 climate scenarios for the discharge of the Rhine and Meuse : comparison with earlier scenario studies*. Deltares Report 1220042-000-ZWS-0004, Delft, The Netherlands, 2015.
- [30] H.F.P. Van den Boogaard, M. Hegnauer, and J.J. Beersma. *GRADE Uncertainty Analysis*. Deltares Report 1209424-004-ZWS-0003, Delft, The Netherlands, 2014.
- [31] S.C. Van Pelt, J. J. Beersma, T.A. Buishand, B.J.J.M. Van den Hurk, and P. Kabat. *Future changes in extreme precipitation in the Rhine basin based on global and regional climate model simulations*. European Geosciences Union (EGU); Copernicus, 2012.
- [32] Detlef P. Van Vuuren, Jae Edmonds, Mikiko Kainuma, Keywan Riahi, Allison Thomson, Kathy Hibbard, George C. Hurtt, Tom Kram, Volker Krey, Jean-Francois Lamarque, Toshihiko Masui, Malte Meinshausen, Nebojsa Nakicenovic, Steven J. Smith, and Steven K. Rose. The representative concentration pathways: an overview. *Climatic Change*, 109:5–31, 2011.
- [33] J.K. Vrijling, W. van Hengel, and R.J. Houben. A framework for risk evaluation. *Journal of Hazardous Materials*, (43):245–261, 1995.